Massive centriole production can occur in the absence of deuterosomes in multiciliated cells

Olivier Mercey, Michelle S Levine, Gina M Lomastro, Philippe Rostaing, Eva Brotslaw, Valerie Gomez, Abhijay Kumar, Nathalie Spassky, Brian J Mitchell, Alice Meunier, et al.

ARTICLES
https://doi.org/10.1038/s41556-019-0427-x
nature cell biology

Massive centriole production can occur in the absence of deuterosomes in multiciliated cells

Olivier Mercey[1,4], Michelle S. Levine[2,4], Gina M. LoMastro[2], Philippe Rostaing[1], Eva Brotslaw[3], Valerie Gomez[2], Abhijay Kumar[2], Nathalie Spassky[1], Brian J. Mitchell[3], Alice Meunier[1,5*] and Andrew J. Holland[2,5*]

Multiciliated cells (MCCs) amplify large numbers of centrioles that convert into basal bodies, which are required for producing multiple motile cilia. Most centrioles amplified by MCCs grow on the surface of organelles called deuterosomes, whereas a smaller number grow through the centriolar pathway in association with the two parent centrioles. Here, we show that MCCs lacking deuterosomes amplify the correct number of centrioles with normal step-wise kinetics. This is achieved through a massive production of centrioles on the surface and in the vicinity of parent centrioles. Therefore, deuterosomes may have evolved to relieve, rather than supplement, the centriolar pathway during multiciliogenesis. Remarkably, MCCs lacking parent centrioles and deuterosomes also amplify the appropriate number of centrioles inside a cloud of pericentriolar and fibrogranular material. These data show that the centriole number is set independently of their nucleation platforms and suggest that massive centriole production in MCCs is a robust process that can self-organize.

Multiciliated cells (MCCs) contain tens of motile cilia that beat to drive fluid flow across epithelial surfaces. Multiciliated cells are present in the respiratory tract, brain ventricles and reproductive systems. Defects in motile-cilia formation or beating lead to the development of hydrocephaly, lethal respiratory symptoms and fertility defects[1–4].

A centriole, or basal body, serves as a template for the cilium axoneme. Centriole duplication is tightly controlled in cycling cells so that a single new procentriole forms adjacent to each of the two parent centrioles[5]. However, MCC progenitors with two parent centrioles produce tens to hundreds of additional new centrioles to nucleate multiple motile cilia[1]. Steric constraints imposed by the 'centriolar' pathway seem to restrict the number of procentrioles that can be nucleated by the parent centrioles. Centriole amplification is therefore thought to rely on the assembly of dozens of MCC-specific organelles called deuterosomes, which each nucleate tens of procentrioles[6–14].

Deuterosomes are assembled during centriole amplification and support the growth of approximately 90% of the procentrioles formed in mammalian MCCs[12,14]. Deuterosomes have been proposed to be nucleated from the younger parent centriole[12] but can form spontaneously in a cloud of pericentriolar material (PCM) in MCCs depleted of the parent centrioles[15–17]. Many of the proteins required for centriole formation in MCCs are common to centriole duplication[11–15,18–23]. However, DEUP1 (*CCDC67*, alternate gene name) has been identified as a deuterosome-specific protein that arose from a gene-duplication event of the centriolar gene *Cep63*. Recent data suggest that *Deup1* evolved to enable the formation of deuterosomes and the generation of large numbers of centrioles[14].

In this manuscript, we interrogate the function of the deuterosome in MCCs from mouse and from *Xenopus laevis*. Surprisingly, our findings reveal that deuterosomes are dispensable for centriole amplification and multiciliogenesis both in vitro and in vivo. Moreover, we show that neither deuterosomes nor parent centrioles are required for MCCs to amplify the correct number of centrioles. These findings raise new questions about the evolutionary role of deuterosome during multiciliogenesis and the mechanisms regulating centriole number in MCCs.

Results

Generation of a *Deup1*-knockout mouse. To examine the role of the deuterosome in multiciliogenesis we created a *Deup1*-knockout mouse by replacing a region from within exon 2 to within exon 7 of the *Deup1* gene with a LacZ reporter (Extended Data Fig. 1a). Reverse Transcription-quantitative PCR on brain and testes samples showed that the messenger RNA levels of *Deup1* were reduced by at least tenfold in *Deup1*-knockout compared with control mice (Extended Data Fig. 1b,c).

To examine the process of multiciliogenesis in *Deup1*$^{-/-}$ cells, we utilized in vitro cultures of mouse tracheal epithelial cells (mTECs) or ependymal cells[24,25]. Consistent with the absence of *Deup1* mRNA, DEUP1 foci were absent in differentiating *Deup1*$^{-/-}$ tracheal cells (Extended Data Fig. 1d). Moreover, full-length DEUP1 protein was undetectable by immunoblot in differentiating *Deup1*$^{-/-}$ ependymal and mTECs (Extended Data Fig. 1e). An in-frame ATG is present near the start of exon 8 of the *Deup1* gene. Although our antibody recognized both the full-length DEUP1 and the exon 8–12 DEUP1 protein fragment ectopically expressed in HEK293FT cells (Extended Data Fig. 1f,g), neither were detectable in the cell lysates of differentiating *Deup1*$^{-/-}$ mouse tracheal or ependymal cells. We thus conclude that *Deup1*$^{-/-}$ mice are null for the DEUP1 protein.

***Deup1*$^{-/-}$ mice lack deuterosomes.** The *Deup1*$^{-/-}$ mice were born at normal Mendelian ratios and had no apparent phenotype

[1]Institut de Biologie de l'ENS (IBENS), CNRS, Inserm, Ecole Normale Supérieure, PSL Research University, Paris, France. [2]Department of Molecular Biology and Genetics, Johns Hopkins University School of Medicine, Baltimore, MD, USA. [3]Department of Cell and Molecular Biology, Feinberg School of Medicine, Northwestern University, Chicago, IL, USA. [4]These authors contributed equally: Olivier Mercey, Michelle S. Levine. [5]These authors jointly supervised this work: Alice Meunier, Andrew J. Holland. *e-mail: alice.meunier@ens.fr; aholland@jhmi.edu

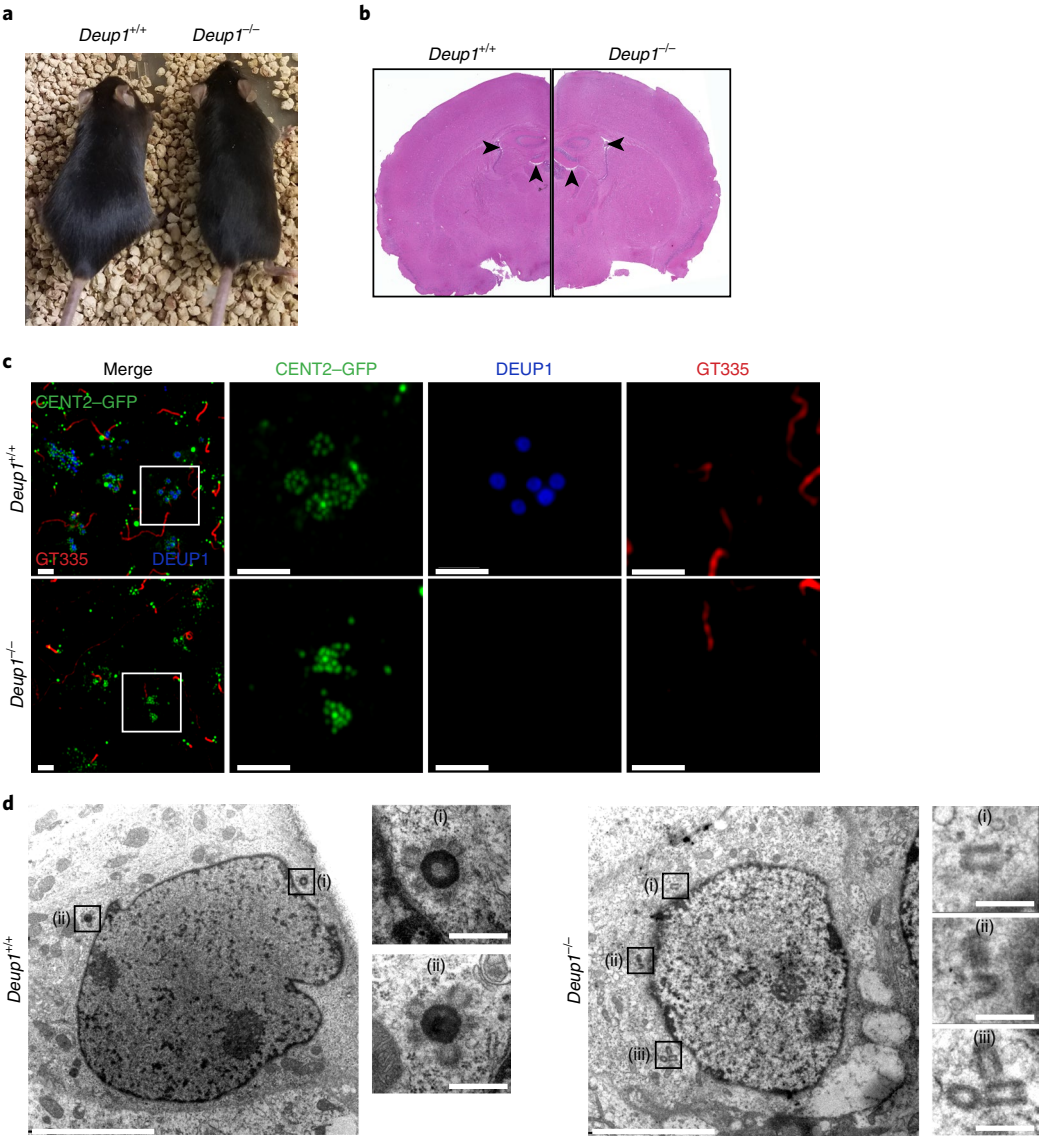

Fig. 1 | *Deup1*-knockout mice lack deuterosomes. a, Images of 5-month-old *Deup1*$^{+/+}$ and *Deup1*$^{-/-}$ mice. **b**, Histological sections from the brains of adult *Deup1*$^{+/+}$ and *Deup1*$^{-/-}$ mice. The arrowheads mark the lateral and third ventricles. Note that there is no apparent hydrocephalus in the *Deup1*$^{-/-}$ mice. **c**, Immunofluorescence images of CENT2–GFP-expressing *Deup1*$^{+/+}$ and *Deup1*$^{-/-}$ ependymal cells in vivo. Brain sections were stained with antibodies against GT335 to mark cilia and DEUP1 to mark the deuterosome. Scale bars, 2 µm. **d**, TEM images of *Deup1*$^{+/+}$ and *Deup1*$^{-/-}$ ependymal cells in the growth stage. Deuterosomes are clearly observed in the cytoplasm ((i) and (ii)) of *Deup1*$^{+/+}$ cells. Deuterosomes were not detected in *Deup1*$^{-/-}$ cells. Instead, singlets (i), doublets (ii) and groups (iii) of procentrioles are observed in the cytoplasm. Scale bars, 5 µm (main images) and 500 nm (zoomed-in regions of interest).

(Supplementary Table 1 and Fig. 1a,b). We analysed the ventricular walls of mouse brains at postnatal days 3–4 (P3–P4) when ependymal progenitor cells differentiate into MCCs to determine whether *Deup1*$^{-/-}$ MCCs lack deuterosomes. Although DEUP1 rings decorated with centrin-stained procentrioles were observed in differentiating *Deup1*$^{+/+}$ ependymal cells, DEUP1 foci were absent from the ventricular walls of *Deup1*$^{-/-}$ brains (Fig. 1c). To confirm the lack of deuterosomes in *Deup1*$^{-/-}$ cells, we performed serial transmission electron microscopy (TEM) through the volume of 11 differentiating *Deup1*$^{-/-}$ ependymal cells cultured in vitro. Although cytoplasmic procentrioles were observed growing from deuterosomes in all of the *Deup1*$^{+/+}$ ependymal cells analysed, procentrioles were never found associated with deuterosomes in the cytoplasm of *Deup1*$^{-/-}$ cells (Fig. 1d). These data show that deuterosomes are absent in *Deup1*$^{-/-}$ mice and confirm previous findings that DEUP1 is a critical structural component of the deuterosome[14].

Deuterosomes are dispensable for centriole amplification during multiciliogenesis. To investigate the role of deuterosomes during centriole amplification in MCCs, we examined the number of centrioles in mature MCCs. Surprisingly, the knockout of *Deup1* did not significantly reduce the number of centrioles formed in multiciliated ependymal or tracheal cells in vitro (Fig. 2a,b and Extended Data Fig. 2a,b). Consistent with our in vitro results, the number of centrioles produced in ependymal cells in the brains of *Deup1*$^{+/+}$ and *Deup1*$^{-/-}$ mice were comparable (Fig. 2c,d). In addition, scanning electron microscopy (SEM) of mouse trachea revealed no differences in the multiciliated epithelium in *Deup1*$^{-/-}$ animals compared with control mice (Fig. 2e).

We examined the effects of Deup1 depletion in MCCs from the *Xenopus* embryonic epidermis to test the requirement of DEUP1 for centriole amplification in a different vertebrate model. Due to the absence of an antibody against *Xenopus* Deup1, we validated

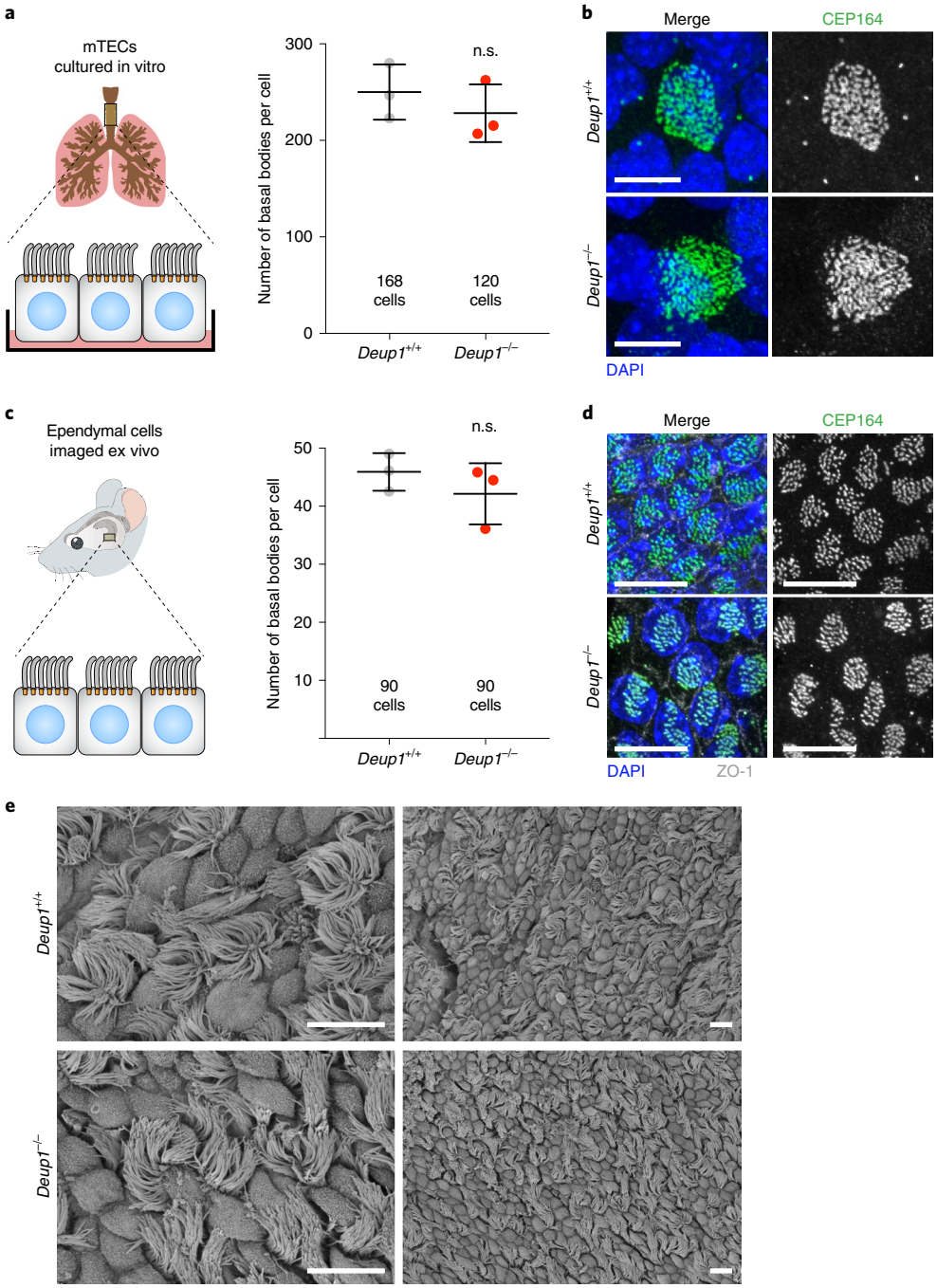

Fig. 2 | Deuterosomes are dispensable for centriole amplification during multiciliogenesis. a, Schematic of mouse lung and harvested mTECs grown in the cell culture experiment (left). Number of basal bodies in mTECs of *Deup1*$^{+/+}$ and *Deup1*$^{-/-}$ mice (right). The basal bodies were stained with CEP164. **b**, Representative images of CEP164-stained basal bodies of *Deup1*$^{+/+}$ and *Deup1*$^{-/-}$ mTECs. Scale bars, 5 µm. **c**, Schematic of mouse brain and harvested ependymal cells grown in the cell culture experiment (right). Number of foci of the basal body marker CEP164 in ependymal cells from *Deup1*$^{+/+}$ and *Deup1*$^{-/-}$ adult-brain sections (right). For **a**,**c**, the total number of cells analysed per genotype is indicated. The bars represent the mean ± s.d.; n.s., not statistically significant ($P > 0.05$); two-tailed unpaired Welch's *t*-test; $n = 3$ mice per genotype. **d**, Representative images of ependymal cells in adult-brain sections from *Deup1*$^{+/+}$ and *Deup1*$^{-/-}$ mice. DAPI marks the nuclei, ZO-1 marks tight junctions and CEP164 stains basal bodies. Scales bars, 10 µm. **e**, SEM images of the tracheas of *Deup1*$^{+/+}$ or *Deup1*$^{-/-}$ adult mice. Scale bars, 10 µm.

the ability of a Deup1 morpholino oligonucleotide to efficiently silence the expression of an mRNA encoding a *Deup1*–green fluorescent protein (GFP) reporter in MCCs (Extended Data Fig. 2c). Importantly, injection of the Deup1 morpholino oligonucleotide did not significantly decrease the number of centrioles generated in *Xenopus* MCCs (Extended Data Fig. 2d,e). These data suggest that Deup1 is not required to amplify the correct number of centrioles in the MCCs of both *Xenopus* and mice.

Our observations contrast those of a previous report that observed a reduction in centriole production after acute depletion of DEUP1 with a short hairpin RNA (shRNA) in mTECs[14]. To address a possible difference in the effect of chronic versus acute

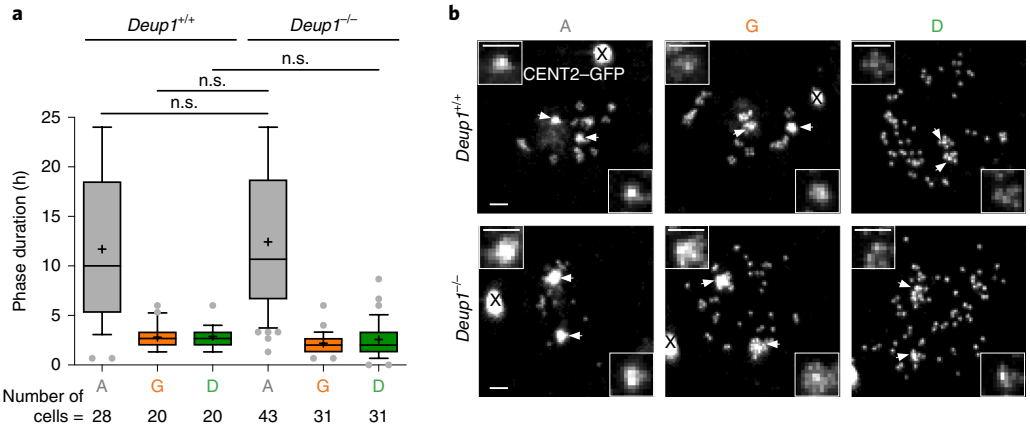

Fig. 3 | Live imaging of differentiating *Deup1*$^{-/-}$ ependymal cells reveals normal step-wise kinetics of centriole amplification. a, Box (25 to 75%)-and-whisker (10 to 90%) plots of the duration of the A, G and D phases in differentiating CENT2-GFP *Deup1*$^{+/+}$ and *Deup1*$^{-/-}$ ependymal cells, determined using time-lapse microscopy. The total number of cells per genotype at each phase is indicated; $n > 3$ cultures per genotype; n.s., not statistically significant ($P > 0.05$); two-tailed unpaired Welch's *t*-test. Lines indicate medians, and crosses indicate means. **b**, Still images from time-lapse videos of CENT2-GFP *Deup1*$^{+/+}$ (Supplementary Video 1) and *Deup1*$^{-/-}$ (Supplementary Video 2) ependymal cells in the A, G and D phases. The arrowheads mark the parent centrioles, which are also shown in zoomed-in images on the top left and bottom right of each image. CENT2-GFP aggregates resulting from expression of the CENT2-GFP transgene[26] are marked with an X. Scale bars, 2 µm. A, amplification phase; G, growth phase and D, disengagement phase. Note that the contrast has been decreased in the zoomed in images to avoid saturation of the signal of the centriolar pathway.

depletion of DEUP1, we used pooled of four short interfering RNAs (siRNAs) to knockdown *Deup1* expression in ependymal cell cultures and analysed the centriole number in cells at the disengagement phase[12] depleted of DEUP1 (Extended Data Fig. 3a,b). Consistent with the results observed in *Deup1*$^{-/-}$ mice, the cells depleted of DEUP1 amplified comparable numbers of centrioles (Extended Data Fig. 3c,d).

Procentrioles form with normal step-wise dynamics in cells lacking deuterosomes. To determine the dynamics of centriole amplification in the absence of deuterosomes, we performed live imaging in differentiating control and *Deup1*$^{-/-}$ ependymal cells expressing GFP-tagged centrin 2 (CENT2–GFP)[26]. It was previously established that centriole amplification proceeds through three stages: amplification, growth and disengagement[12,19]. Each of these phases of centriole amplification was distinguishable in both *Deup1*$^{+/+}$ and *Deup1*$^{-/-}$ cells (Supplementary Videos 1 and 2), and the loss of DEUP1 did not affect their duration (Fig. 3a).

The amplification stage in *Deup1*$^{+/+}$ ependymal MCCs is marked by the emergence of CENT2–GFP rings representing procentrioles organized around deuterosomes (Fig. 3b, top row and Supplementary Video 1)[12,17]. In contrast, CENT2–GFP rings were not observed in *Deup1*$^{-/-}$ cells. Instead, the cells exhibited an increased CENT2–GFP signal around the parent centrioles and a gradual accumulation of faint CENT2–GFP foci arising from a region close to the parent centrioles (Fig. 3b, bottom row and Supplementary Video 2). The CENT2–GFP rings transformed into flower-like structures in control cells during the growth stage, reflecting the growth of procentrioles associated with deuterosomes (Fig. 3b, top row and Supplementary Video 1). The CENT2–GFP signal around the parent centrioles in *Deup1*$^{-/-}$ cells developed into brighter CENT2–GFP spots, showing that the amplification of centrioles via the centriolar pathway is increased in cells lacking deuterosomes. The faint cytoplasmic CENT2–GFP foci in *Deup1*$^{-/-}$ cells also resolved into distinct CENT2–GFP spots, which represent single or small groups of procentrioles (Fig. 3b, bottom row and Supplementary Video 2). At the disengagement stage, centrioles were simultaneously released from deuterosomes and parent centrioles in control cells and from the parent centrioles and small groups of procentrioles in *Deup1*$^{-/-}$ cells. We conclude that *Deup1*$^{-/-}$ cells achieve the correct number of centrioles through the normal step-wise dynamics of centriole amplification. Nevertheless, *Deup1*$^{-/-}$ cells differ from control cells in two important characteristics: first, the centriolar pathway is increased in *Deup1*$^{-/-}$ cells and second, the procentrioles that are present in the cytoplasm are organized into smaller groups that do not adopt a ring-shaped morphology.

Procentrioles form in the vicinity of the parent centrioles in the absence of deuterosomes. We performed super-resolution imaging of differentiating ependymal cells lining the ventricular walls of the brain to increase the spatial resolution of our analysis. Whereas SAS6^{+} procentrioles were observed growing from both deuterosomes and parent centrioles during the amplification stage in control cells, SAS6^{+} procentrioles were observed on the wall of parent centrioles and scattered in the vicinity of these structures in the brains of *Deup1*$^{-/-}$ mice (Fig. 4a). An increase in SAS6 staining at the parent centrioles in *Deup1*$^{-/-}$ cells confirmed that more procentrioles are nucleated by parent centrioles compared with controls (Fig. 4a and Extended Data Fig. 4b). We observed a preferential localization of SAS6 to the younger parent centriole compared with the older centriole (distinguishable in the amplification stage by the presence of a cilium) in both *Deup1*$^{+/+}$ and *Deup1*$^{-/-}$ cells (Fig. 4a and Extended Data Fig. 4a). This asymmetry in SAS6 staining suggests that the younger parent centriole has a greater capacity for procentriole nucleation[12]. Consistent with the live imaging, the procentrioles that were present in the cytoplasm of *Deup1*$^{-/-}$ cells were more widely distributed during the growth stage than in the amplification stage and were organized as singlets or small groups of procentrioles (Fig. 4a). These data suggest that in the absence of deuterosomes, most procentrioles are formed on the wall of the parent centrioles and in their vicinity before being released into the cytoplasm.

We performed serial-section electron microscopy or correlative light and electron microscopy (CLEM) on cultured ependymal cells during the growth stage to resolve procentriole formation that occurs close to the parent centrioles. As expected, the majority of procentrioles formed on the surface of deuterosomes and small numbers were present on the parent centrioles in *Deup1*$^{+/+}$ cells (Fig. 4b and Supplementary Video 3). Interestingly, we observed that more procentrioles were produced on the surface of the parent centrioles in *Deup1*$^{-/-}$ cells (Fig. 4c, Extended Data Fig. 4c and

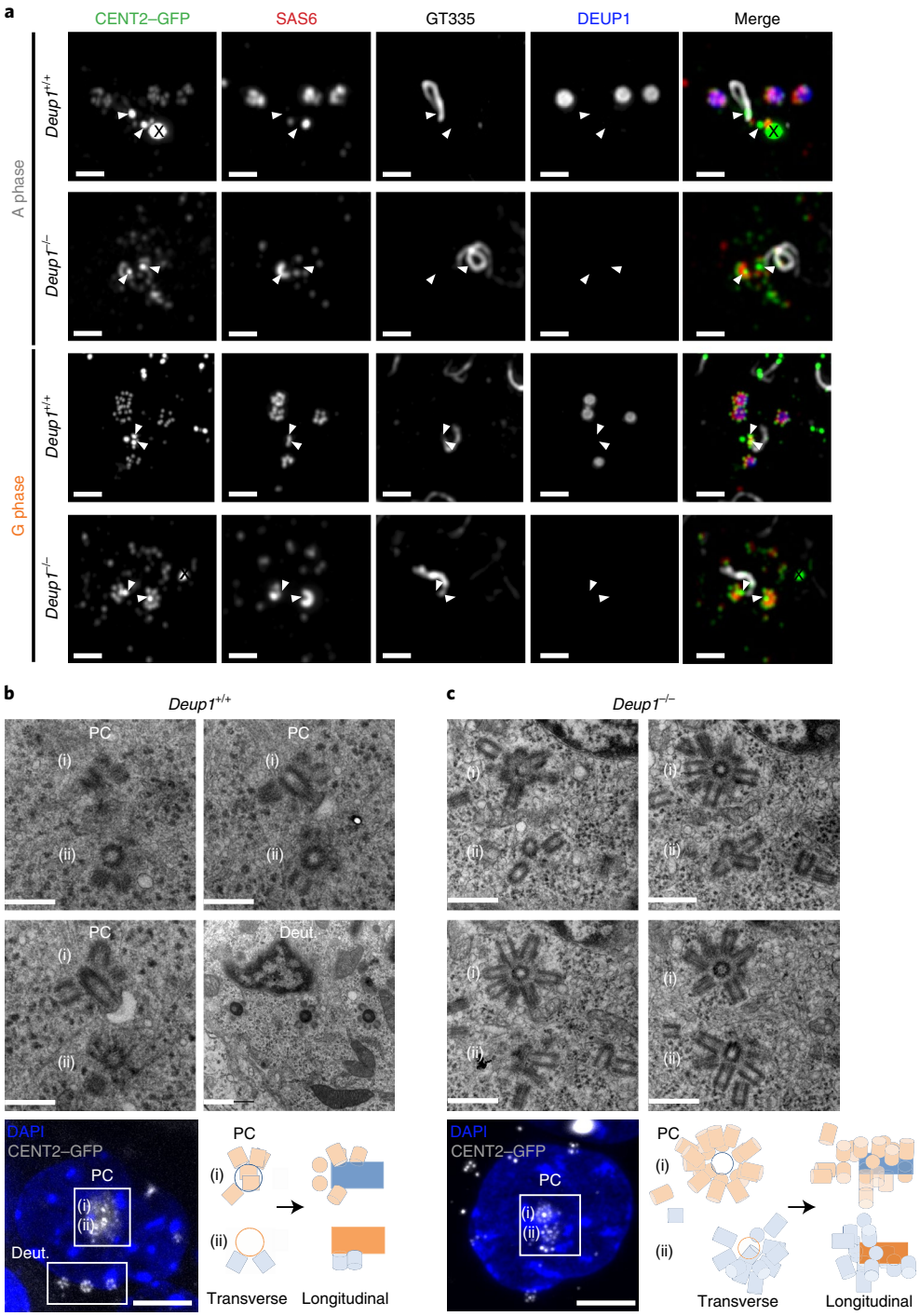

Fig. 4 | Centriole amplification in the absence of deuterosomes occurs on and in proximity to pre-existing centrioles. a, Immunofluorescence images of CENT2–GFP-expressing *Deup1*$^{+/+}$ and *Deup1*$^{-/-}$ ependymal cells in vivo (P2–P6). Brain sections were stained with antibodies against GT335, SAS6 and DEUP1. GT335 marks the cilium that forms from the older parent centriole, SAS6 marks the new procentrioles and DEUP1 marks the deuterosome. The CENT2–GFP aggregates resulting from the expression of the CENT2–GFP transgene[26] are indicated with an X. The arrowheads indicate the location of pre-existing centrioles. Scale bars, 2 µm. **b**, CLEM images of a CENT2–GFP-expressing *Deup1*$^{+/+}$ ependymal cell in the growth phase (top and middle). Procentrioles are formed by both parent centrioles (PC) and deuterosomes (Deut.). Immunofluorescence image of the CENT2–GFP *Deup1*$^{+/+}$ cell depicted in the electron microscopy images (bottom left). Schematic representation of the relative position of procentrioles formed on the parent centrioles (bottom right). Scale bars, 600 nm (CLEM) and 5 µm (immunofluorescence). Note that images are taken from the same cell as that in Fig. 1d *Deup1*$^{+/+}$. Serial z-sections of this cell are shown in Supplementary Video 3. **c**, CLEM images of a CENT2–GFP-expressing *Deup1*$^{-/-}$ cell in the growth phase reveals centriole amplification on, or in close proximity to, the parent centrioles (top and middle). Procentrioles are also observed further away in the cytoplasm. Immunofluorescence image of the CENT2–GFP *Deup1*$^{-/-}$ cell depicted in the electron microscopy images (bottom left). Schematic representation of the relative position of procentrioles formed on the parent centrioles (bottom right). Scale bars, 600 nm (CLEM) and 5 µm (immunofluorescence). Note that images are taken from the same cell as that in Fig. 1d *Deup1*$^{-/-}$. Serial z-sections of this cell are shown in Supplementary Video 4. Three dimensional reconstruction of the parent centrioles is shown in Supplementary Video 5.

Supplementary Video 4). Whereas procentrioles were predominantly nucleated from the proximal end of the parent centrioles in control cells, they could form along the entire length of the parent centrioles in *Deup1*$^{-/-}$ cells, allowing the growth of up to 18 procentrioles from a single parent centriole (Fig. 4c, Extended Data Fig. 4c and Supplementary Video 5). Consistent with live-cell imaging and ex vivo analysis, singlets or groups of 2 or 3 procentrioles, which were often connected at their proximal side, were also observed in the vicinity of the parent centrioles and further away in the cytoplasm (Figs. 1d, 4c and Extended Data Fig. 4c). These groups of procentrioles could be observed around the nuclear membrane during the growth phase (Supplementary Video 4). We conclude that in the absence of deuterosomes, the centriolar pathway is enhanced and procentrioles form along the entire length and in the vicinity of the parent centrioles. As the amplification stage progresses, singlets or groups of procentrioles are released into the cytoplasm and are organized around the nuclear envelope in a similar configuration to that seen in control cells[17,19].

Despite the increase in nucleation of procentrioles on the parent centrioles, incomplete rings of SAS6 were often observed around the circumference of parent centrioles in *Deup1*$^{-/-}$ cells (Fig. 4a) and sites unoccupied by procentrioles were also visible on the walls of the parent centrioles by electron microscopy (Fig. 4c, Extended Data Fig. 4c and Supplementary Videos 4,5). This non-homogenous distribution may arise as a result of a symmetry-breaking reaction that creates a non-uniform distribution of PLK4, similar to what occurs in cycling cells[27]. Alternatively, procentrioles may detach from the walls of the parent centrioles, which could explain their presence in close proximity to the parent centrioles (Fig. 4a,c and Extended Data Fig. 4c).

CEP63 loss modestly reduces centriole amplification in *Deup1*$^{-/-}$ MCCs. *Deup1* is a paralogue of the centriolar protein encoding gene *Cep63*. The two proteins share 37% sequence identity in mice and compete for binding to the centriole duplication protein CEP152 (ref. [14]). It has been proposed that CEP63 could compensate for the loss of DEUP1 by enhancing the recruitment of CEP152 to the parent centrioles to trigger increased procentriole nucleation[14]. Importantly, the level of *Cep63* mRNA in whole-culture extracts and CEP63 protein in single cells in the process of centriole amplification was unchanged in *Deup1*$^{-/-}$ cells (Extended Data Fig. 5a,b). We obtained *Cep63*$^{T/T}$ mice, which have the *Cep63* gene disrupted with a gene-trap insertion[28,29]. *Cep63*$^{T/T}$ mice showed a >40-fold reduction in the levels of *Cep63* mRNA in mouse testes and mTECs (Extended Data Fig. 5c). The loss of *Cep63* expression did not decrease the final number of centrioles produced in fully differentiated mTECs or ependymal cells in vitro or in vivo (Extended Data Fig. 5d–i). Analysis by SEM of trachea revealed no apparent defect in multiciliogenesis in *Deup1*$^{-/-}$; *Cep63*$^{T/T}$ mice compared with controls (Extended Data Fig. 5j). In addition, the morpholino-oligonucleotide-mediated depletion of both Cep63 and Deup1 in multiciliated *Xenopus* epithelial cells did not significantly decrease the final number of centrioles generated (Extended Data Fig. 6a–c). However, *Deup1*$^{-/-}$; *Cep63*$^{T/T}$ ependymal cells analysed ex vivo showed a 22% decrease in the number of centrioles amplified compared with controls (Extended Data Fig. 5h,i). Although not statistically significant, we also noted a modest decrease in centriole number in *Deup1*$^{-/-}$; *Cep63*$^{T/T}$ ependymal cells (10%) and mTECs (18%) differentiated in vitro (Extended Data Fig. 5d–g). These data show that CEP63 may modestly compensate for the loss of *Deup1*.

Loss of *Deup1* does not compromise basal-body symmetry or cilia function. We performed TEM on fully differentiated cultured ependymal MCCs to analyse the core structure of basal bodies that assemble in *Deup1*$^{-/-}$ and *Deup1*$^{-/-}$; *Cep63*$^{T/T}$ MCCs. More than 95% of the mature basal bodies in *Deup1*$^{+/+}$, *Deup1*$^{-/-}$ and *Deup1*$^{-/-}$; *Cep63*$^{T/T}$ MCCs exhibited a normal cylindrical structure (Extended Data Fig. 6d–e). Higher resolution TEM analysis on transversally sectioned basal bodies and cilia revealed no increase in 9-fold symmetry defects of basal bodies or in structural abnormalities of cilia in *Deup1*$^{-/-}$ and *Deup1*$^{-/-}$; *Cep63*$^{T/T}$ MCCs compared with control cells (Fig. 5a–d). The lengths of the mature basal bodies were similar in control and *Deup1*$^{-/-}$ ependymal cells but about 7% longer in the *Deup1*$^{-/-}$; *Cep63*$^{T/T}$ MCCs (Fig. 5e). *Deup1*$^{-/-}$ and *Deup1*$^{-/-}$; *Cep63*$^{T/T}$ ependymal cells produced cilia that beat with similar frequencies to that observed in control cells (Fig. 5f and Supplementary Videos 6–8). Finally, the lengths of the cilia that formed in vivo—measured by SEM of trachea—were comparable in control, *Deup1*$^{-/-}$ and *Deup1*$^{-/-}$; *Cep63*$^{T/T}$ cells (Fig. 5g). Together, these data suggest that deuterosomes are not required to produce structurally sound basal bodies and functional cilia.

Centriole amplification can occur without deuterosomes and parent centrioles. We interrogated the role of parent centrioles in promoting centriole amplification in *Deup1*$^{+/+}$ and *Deup1*$^{-/-}$ cells. Recent work has shown that the treatment of cycling MCC progenitor cells with the PLK4 inhibitor centrinone depletes parent centrioles but does not prevent deuterosome formation during MCC differentiation[15–17,30]. We obtained a mixed population of cells with two, one or zero parent centrioles by treating ependymal progenitors with centrinone during their proliferation. Multiciliated cell differentiation was then triggered after centrinone washout and centriole amplification was monitored by single live-cell imaging in CENT2–GFP-expressing *Deup1*$^{+/+}$ and *Deup1*$^{-/-}$ cells that lacked parent centrioles. Remarkably, as previously described in *Deup1*$^{+/+}$ cells[17], the loss of parent centrioles did not prevent centriole amplification in *Deup1*$^{-/-}$ ependymal cells (Fig. 6a and Supplementary Videos 9,10). In addition, the final number of centrioles produced in *Deup1*$^{-/-}$ cells lacking parent centrioles was similar to that in *Deup1*$^{-/-}$ cells with two parent centrioles (Fig. 6b). These data suggest that massive centriole amplification can occur without deuterosomes and parent centrioles in mouse MCCs.

Procentrioles are amplified within the confines of a PCM cloud. Immunofluorescence staining of in vivo and in vitro differentiating ependymal MCCs in the amplification and growth phases suggested that procentrioles were largely amplified within the confines of a cloud marked by the PCM protein pericentrin (PCNT; Fig. 6c,d and Extended Data Fig. 7a,b). This preferential localization of newborn procentrioles occurred whether or not deuterosomes or parent centrioles were present. The abundance and size of the PCNT cloud was unaltered by the absence of deuterosomes and parent centrioles (Extended Data Fig. 7c,d). To further analyse how centrioles are amplified in the absence of both parent centrioles and deuterosomes, we performed CLEM on a *Deup1*$^{-/-}$ ependymal cell that lacked parent centrioles during the amplification or growth phases. We observed single or small groups of procentrioles in a nuclear pocket where fibrogranular material was concentrated[6,8,31] (Fig. 6e and Supplementary Videos 11,12). This suggests that the minimal micro-environment for centriole biogenesis and number control in MCCs does not require the deuterosome or parent centrioles and is instead characterized by a proximity to the nuclear membrane and the presence of PCM and fibrogranular material.

Discussion

In this manuscript, we show that deuterosomes are dispensable for procentriole amplification during multiciliogenesis. Cells that lack deuterosomes amplify the correct number of centrioles through apparently normal step-wise kinetics. This amplification occurs through the production of procentrioles in high numbers in the vicinity and along the entire length of the parent centrioles, suggesting that deuterosome organelles have evolved to relieve rather

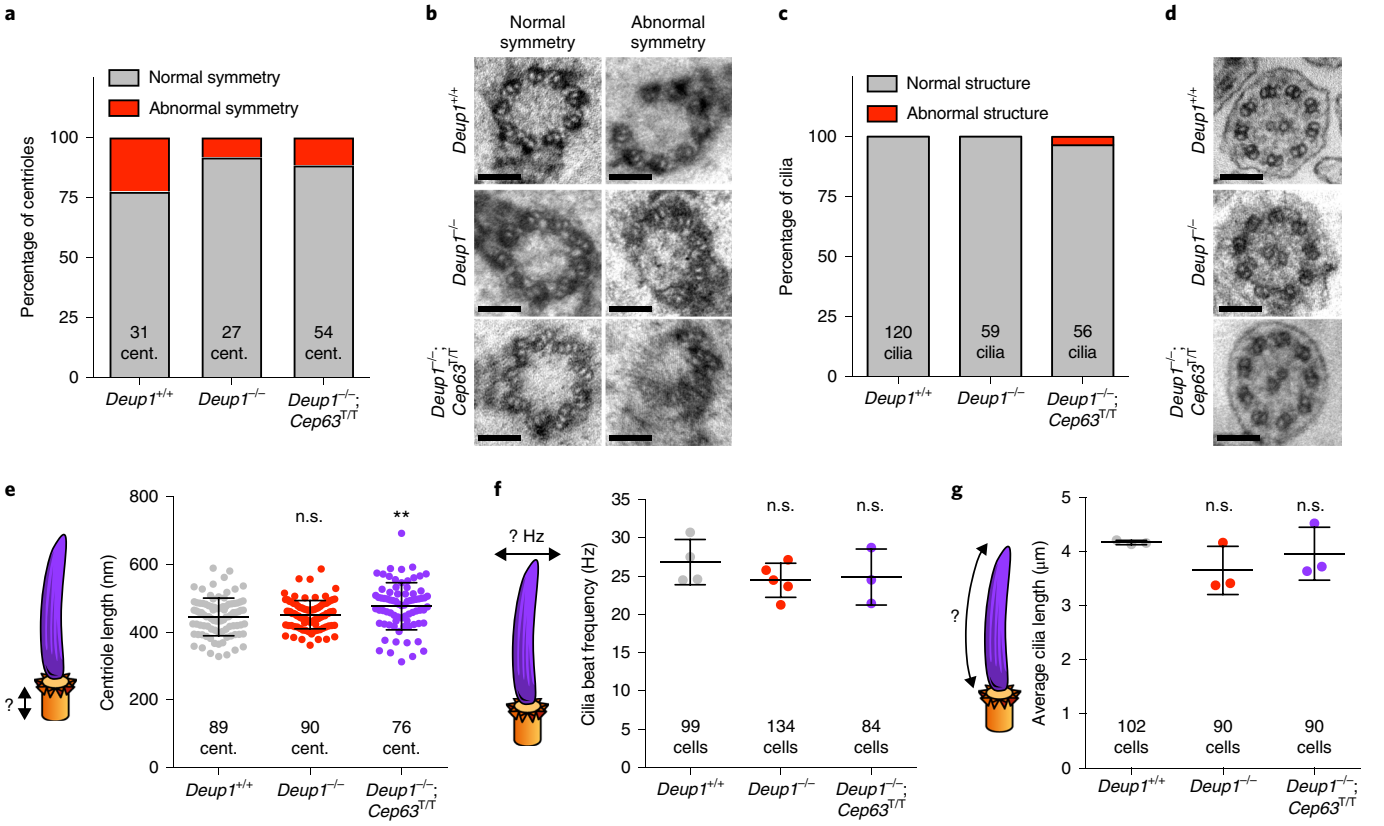

Fig. 5 | The loss of *Deup1* does not compromise basal-body symmetry or cilia function. a, Percentage of centrioles in *Deup1*$^{+/+}$, *Deup1*$^{-/-}$ and *Deup1*$^{-/-}$; *Cep63*$^{T/T}$ ependymal cells with abnormal symmetry in vitro. The total number of centrioles (cent.) analysed per genotype is indicated; $n > 10$ cells per genotype. **b**, Representative TEM images of both normal and abnormal symmetry observed in the centrioles of *Deup1*$^{+/+}$, *Deup1*$^{-/-}$ and *Deup1*$^{-/-}$; *Cep63*$^{T/T}$ ependymal cells in vitro. Scale bars, 100 nm. **c**, Percentage of cilia with abnormal structure in fully differentiated *Deup1*$^{+/+}$, *Deup1*$^{-/-}$ and *Deup1*$^{-/-}$; *Cep63*$^{T/T}$ ependymal cells in vitro. The total number of cilia analysed per genotype is indicated; $n > 5$ cells per genotype. **d**, Representative TEM images of the structure of normal cilia in fully differentiated *Deup1*$^{+/+}$, *Deup1*$^{-/-}$ and *Deup1*$^{-/-}$; *Cep63*$^{T/T}$ ependymal cells in vitro. Scale bars, 100 nm. **e**, Lengths of the centrioles, determined using TEM, of fully differentiated *Deup1*$^{+/+}$, *Deup1*$^{-/-}$ and *Deup1*$^{-/-}$; *Cep63*$^{T/T}$ ependymal cells. Each point represents a single centriole. The total number of centrioles analysed per genotype is indicated; $n > 10$ cells per genotype. **f**, Ciliary beat frequency in fully differentiated *Deup1*$^{+/+}$, *Deup1*$^{-/-}$ and *Deup1*$^{-/-}$; *Cep63*$^{T/T}$ ependymal cells. The total number of cells analysed per genotype is indicated; $n \geq 3$ cultures per genotype. **g**, Lengths of the cilia, measured using SEM, of *Deup1*$^{+/+}$, *Deup1*$^{-/-}$ and *Deup1*$^{-/-}$; *Cep63*$^{T/T}$ mTECs in vivo. The total number of cells analysed per genotype is indicated. **e**–**g**, The bars represent the mean ± s.d. $^{**}P \leq 0.01$; n.s., not statistically significant ($P > 0.05$); two-tailed unpaired Welch's *t*-test.

than supplement the centriolar pathway (Extended data Fig. 7e). Remarkably, MCC progenitors still amplify the appropriate number of centrioles within the confines of a cloud of PCM and fibrogranular material in the absence of both deuterosomes and parent centrioles (Extended data Fig. 7e). We conclude that the centriole number is set independently of the centrosome and deuterosome organelles and hypothesize that centriole amplification in MCCs is a robust process supported by the self-assembly properties of centrioles.

A previous study reported that centriole production was reduced by approximately 35% in differentiating mTECs following the stable expression of a *Deup1* shRNA[14]. In contrast, our data demonstrate that the loss of DEUP1, through gene knockout in tracheal and ependymal cells or through siRNA depletion in ependymal cells, does not significantly reduce the final number of centrioles. The reason for this discrepancy may arise from the quantification of centriole number during the growth stage[14], where procentrioles in *Deup1*$^{-/-}$ MCCs are difficult to accurately count due to the upregulation of the centriolar pathway. In contrast, our quantification was performed at the disengagement/multiple basal body stages, where individual centrioles can be better resolved. In the same study[14], Zhao et al. showed that shRNA depletion of both CEP63 and DEUP1 decreased the number of centrioles produced in cultured mTECs by approximately 90%. In our study, we observed only a modest decrease in centriole formation in *Deup1*$^{-/-}$; *Cep63*$^{T/T}$ tracheal and ependymal cells. The involvement of CEP63 in centriole amplification in *Deup1*$^{-/-}$ MCCs requires further investigation.

Although defects in centriole amplification in MCCs can lead to the development of a condition known as reduced generation of motile cilia (RGMC)[32–34], patients with mutations in *DEUP1* have yet to be identified. According to the gnomAD database, 4.7% of Africans are heterozygous for a nonsense mutation in exon 12 of *DEUP1* (p.Arg468Ter), which is predicted to lead to a truncated or absent protein product, and homozygous individuals have not been reported to have symptoms of RGMC[35]. Moreover, our study shows that the kinetics of centriole amplification and centriole number, structure and function seem unaffected by the absence of deuterosomes in mouse MCCs. Finally, flatworms lack *DEUP1* and can produce MCCs with dense multicilia without utilizing deuterosome structures[36,37], which is consistent with deuterosomes being dispensable for centriole amplification. Together, these observations question the nature of the benefit provided by deuterosome organelles, which are widely conserved across vertebrate MCCs.

The centrosomal region becomes densely populated with procentrioles when deuterosomes are absent, suggesting that deuterosomes could help prevent the overcrowding of parent centrioles, which may interfere with other centrosomal functions. DEUP1 interacts

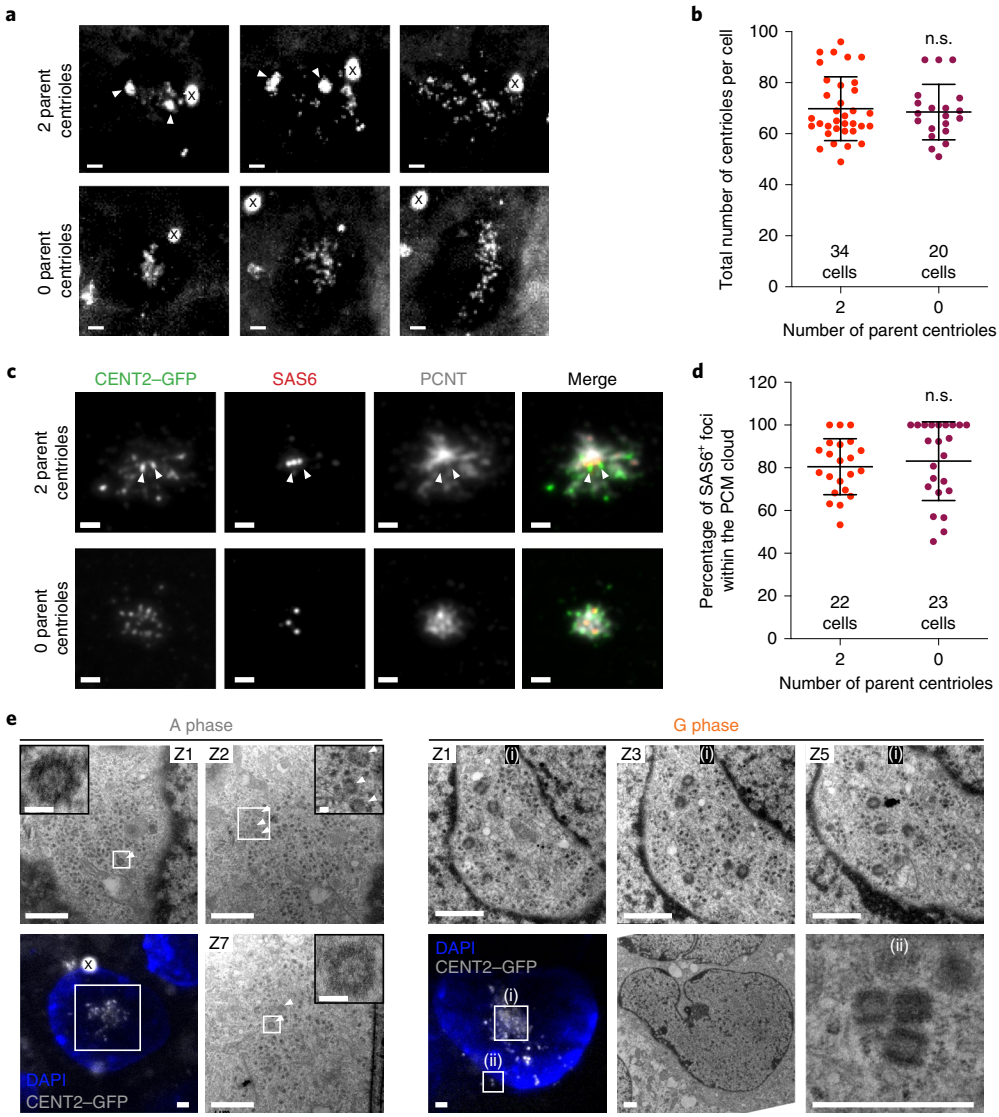

Fig. 6 | Centriole amplification can occur without deuterosomes and parent centrioles. a, Images from videos of CENT2–GFP-expressing *Deup1*$^{-/-}$ ependymal cells transiently treated with centrinone. The images show cells with two (Supplementary Video 9) or zero (Supplementary Video 10) parent centrioles. The phases of centriole amplification cannot be accurately determined in *Deup1*$^{-/-}$ cells with zero parent centrioles. The CENT2–GFP aggregates[26] are indicated with an X. **b**, Number of centrioles in CENT2–GFP-expressing *Deup1*$^{-/-}$ ependymal cells. The quantifications were carried out using time-lapse imaging at the end of amplification in cells that began centriole amplification with two or zero parent centrioles. $n > 3$ cultures per condition. **c**, Immunofluorescence images of cultured CENT2–GFP-expressing *Deup1*$^{-/-}$ ependymal cells treated with centrinone. The images show cells with two or zero parent centrioles. **a**,**c**, The arrowheads mark the parent centrioles, when present. Scale bars, 2 µm. **d**, Percentage of SAS6^{+} foci localized in the PCM cloud in CENT2–GFP-expressing *Deup1*$^{-/-}$ ependymal cells at the beginning of amplification in cells with either two or zero parent centrioles. Quantification is based on the localization of SAS6 foci in the PCM cloud marked by PCNT staining. $n \geq 2$ cultures per condition. **b**,**d**, Each point represents a single cell. The total number of cells analysed is indicated. The bars represent the mean ± s.d.; n.s., not statistically significant ($P > 0.05$); two-tailed unpaired Welch's *t*-test. **e**, CLEM images of CENT2–GFP-expressing *Deup1*$^{-/-}$ ependymal cells treated with centrinone with zero parent centrioles. A cell in the A phase (stage based on the length of the procentrioles, left) and one in the G phase (stage based on the length of the procentrioles, right) are shown (serial sections of these cells shown in Supplementary Videos 11 and 12). The arrowheads mark procentrioles forming in the absence of pre-existing centrioles and deuterosomes. They form as either single free-standing procentrioles (i) or small groups of two or three procentrioles (ii). Scale bars, 1 µm (main images) and 100 nm (zoomed-in regions of interest). Different 70-nm serial z-sections are shown and numbered relatively to each others.

with CEP152 and is capable of self-assembling into deuterosome-like structures when expressed in bacteria[14]. One possibility is that DEUP1 recruits CEP152 and biases centriole nucleation away from the parent centrioles. Alternatively, an interaction with CEP152 could allow DEUP1 to be recruited by procentrioles nucleated on, or in the vicinity of, the parent centrioles. This hypothesis is consistent with the observation that deuterosomes are often found associated with the younger parent centriole and that more procentrioles amplify from this site in *Deup1*$^{-/-}$ cells[12]. In both cases, DEUP1 self-assembly would relieve the centriolar pathway by sequestering procentrioles into groups away from the parent centrioles.

Procentrioles were observed in *Deup1*$^{-/-}$ cells, by electron microscopy and super-resolution imaging of ependymal MCCs, along the entire length of the parent centrioles and in their vicinity. Live imaging of CENT2–GFP and staining of the PCM suggests that these procentrioles are progressively released from the centrosomal

region. How these procentrioles arise remains unclear. One possibility is that all of the centrioles in *Deup1*$^{-/-}$ cells are nucleated on the wall of the parent centrioles but some detach because of ectopic attachment or steric constraints. Another possibility is that some procentrioles are nucleated 'de novo' in the PCM[38]. Finally, we cannot exclude the possibility that procentrioles could also be nucleated by other procentrioles. This is supported by the presence of orthogonal and co-linear configurations of procentrioles in the cytoplasm of *Deup1*$^{-/-}$ cells with or without parent centrioles (Figs. 1e, 4c, 6e and Extended Data Fig. 4c). However, procentrioles engaged in an orthogonal or co-linear configuration have similar lengths, arguing against a reduplication process. Nucleation by centrosomal centrioles, de novo centriole assembly and centriole reduplication have been proposed to contribute jointly to centriole amplification in the MCCs of the *Macrostomum* flatworm, which lacks deuterosomes[36]. In MCCs that lack both centrosomes and deuterosomes, such as in the *Schmidtea mediterranea* flatworm, the mode of centriole amplification is unknown[37].

Our study suggests that the minimal environment for centriole amplification in MCCs does not require deuterosomes or parent centrioles but is characterized by the presence of PCM and fibrogranular material. Notably, fibrogranular material in MCCs was shown to contain the protein PCM1[39], which is also required to scaffold the assembly of the 'pericentriolar satellites' that are found in non-MCCs. It is therefore possible that the fibrogranular material is functionally equivalent to the pericentriolar satellites of non-MCCs[40–43]. Additional studies will be required to identify the minimal components involved in centriole assembly and number control, and to define the role of DEUP1 and the deuterosome in MCCs.

Online content

Any methods, additional references, Nature Research reporting summaries, source data, extended data, supplementary information, acknowledgements, peer review information; details of author contributions and competing interests; and statements of data and code availability are available at https://doi.org/10.1038/s41556-019-0427-x.

Received: 16 April 2019; Accepted: 25 October 2019;
Published online: 2 December 2019

References

1. Spassky, N. & Meunier, A. The development and functions of multiciliated epithelia. *Nat. Rev. Mol. Cell Biol.* **18**, 423–436 (2017).
2. Reiter, J. F. & Leroux, M. R. Genes and molecular pathways underpinning ciliopathies. *Nat. Rev. Mol. Cell Biol.* **18**, 533–547 (2017).
3. Terre, B. et al. Defects in efferent duct multiciliogenesis underlie male infertility in GEMC1-, MCIDAS- or CCNO-deficient mice. *Development* **146**, dev162628 (2019).
4. Yuan, S. et al. Motile cilia of the male reproductive system require miR-34/miR-449 for development and function to generate luminal turbulence. *Proc. Natl Acad. Sci. USA* **116**, 3584–3593 (2019).
5. Nigg, E. A. & Holland, A. J. Once and only once: mechanisms of centriole duplication and their deregulation in disease. *Nat. Rev. Mol. Cell Biol.* **19**, 297–312 (2018).
6. Anderson, R. G. & Brenner, R. M. The formation of basal bodies (centrioles) in the rhesus monkey oviduct. *J. Cell Biol.* **50**, 10–34 (1971).
7. Brenner, R. M. Renewal of oviduct cilia during the menstrual cycle of the rhesus monkey. *Fertil. Steril.* **20**, 599–611 (1969).
8. Sorokin, S. P. Reconstructions of centriole formation and ciliogenesis in mammalian lungs. *J. Cell Sci.* **3**, 207–230 (1968).
9. Steinman, R. M. An electron microscopic study of ciliogenesis in developing epidermis and trachea in the embryo of *Xenopus laevis*. *Am. J. Anat.* **122**, 19–55 (1968).
10. Kalnins, V. I. & Porter, K. R. Centriole replication during ciliogenesis in the chick tracheal epithelium. *Z. Zellforsch. Mikrosk. Anat.* **100**, 1–30 (1969).
11. Revinski, D. R. et al. CDC20B is required for deuterosome-mediated centriole production in multiciliated cells. *Nat. Commun.* **9**, 4668 (2018).
12. Al Jord, A. et al. Centriole amplification by mother and daughter centrioles differs in multiciliated cells. *Nature* **516**, 104–107 (2014).
13. Klos Dehring, D. A. et al. Deuterosome-mediated centriole biogenesis. *Dev. Cell* **27**, 103–112 (2013).
14. Zhao, H. et al. The Cep63 paralogue Deup1 enables massive de novo centriole biogenesis for vertebrate multiciliogenesis. *Nat. Cell Biol.* **15**, 1434–1444 (2013).
15. Zhao, H. et al. Parental centrioles are dispensable for deuterosome formation and function during basal body amplification. *EMBO Rep.* **20**, e46735 (2019).
16. Nanjundappa, R. et al. Regulation of cilia abundance in multiciliated cells. *eLife* **8**, e44039 (2019).
17. Mercey, O. et al. Dynamics of centriole amplification in centrosome-depleted brain multiciliated progenitors. *Sci. Rep.* **9**, 13060 (2019).
18. Vladar, E. K. & Stearns, T. Molecular characterization of centriole assembly in ciliated epithelial cells. *J. Cell Biol.* **178**, 31–42 (2007).
19. Al Jord, A. et al. Calibrated mitotic oscillator drives motile ciliogenesis. *Science* **358**, 803–806 (2017).
20. Wang, L. et al. miR-34b regulates multiciliogenesis during organ formation in zebrafish. *Development* **140**, 2755–2764 (2013).
21. Ma, L., Quigley, I., Omran, H. & Kintner, C. Multicilin drives centriole biogenesis via E2f proteins. *Genes Dev.* **28**, 1461–1471 (2014).
22. Tan, F. E. et al. Myb promotes centriole amplification and later steps of the multiciliogenesis program. *Development* **140**, 4277–4286 (2013).
23. Vladar, E. K. et al. Cyclin-dependent kinase control of motile ciliogenesis. *eLife* **7**, e36375 (2018).
24. You, Y. & Brody, S. L. Culture and differentiation of mouse tracheal epithelial cells. *Methods Mol. Biol.* **945**, 123–143 (2013).
25. Delgehyr, N. et al. Ependymal cell differentiation, from monociliated to multiciliated cells. *Methods Cell Biol.* **127**, 19–35 (2015).
26. Higginbotham, H., Bielas, S., Tanaka, T. & Gleeson, J. G. Transgenic mouse line with green-fluorescent protein-labeled centrin 2 allows visualization of the centrosome in living cells. *Transgenic Res.* **13**, 155–164 (2004).
27. Leda, M., Holland, A. J. & Goryachev, A. B. Autoamplification and competition drive symmetry breaking: initiation of centriole duplication by the PLK4-STIL network. *iScience* **8**, 222–235 (2018).
28. Brown, N. J., Marjanovic, M., Luders, J., Stracker, T. H. & Costanzo, V. Cep63 and cep152 cooperate to ensure centriole duplication. *PLoS ONE* **8**, e69986 (2013).
29. Marjanovic, M. et al. CEP63 deficiency promotes p53-dependent microcephaly and reveals a role for the centrosome in meiotic recombination. *Nat. Commun.* **6**, 7676 (2015).
30. Wong, Y. L. et al. Cell biology. Reversible centriole depletion with an inhibitor of Polo-like kinase 4. *Science* **348**, 1155–1160 (2015).
31. Dirksen, E. R. Centriole morphogenesis in developing ciliated epithelium of the mouse oviduct. *J. Cell Biol.* **51**, 286–302 (1971).
32. Wallmeier, J. et al. Mutations in CCNO result in congenital mucociliary clearance disorder with reduced generation of multiple motile cilia. *Nat. Genet.* **46**, 646–651 (2014).
33. Amirav, I. et al. Systematic analysis of CCNO variants in a defined population: implications for clinical phenotype and differential diagnosis. *Hum. Mutat.* **37**, 396–405 (2016).
34. Boon, M. et al. Primary ciliary dyskinesia: critical evaluation of clinical symptoms and diagnosis in patients with normal and abnormal ultrastructure. *Orphanet J. Rare Dis.* **9**, 11 (2014).
35. Karczewski, K. J. et al. Variation across 141,456 human exomes and genomes reveals the spectrum of loss-of-function intolerance across human protein-coding genes. Preprint at *bioRxiv* https://doi.org/10.1101/531210 (2019).
36. Tyler, S. Development of cilia in embryos of the turbellarian *Macrostomum*. *Hydrobiologia* **84**, 231–239 (1981).
37. Azimzadeh, J., Wong, M. L., Downhour, D. M., Sanchez Alvarado, A. & Marshall, W. F. Centrosome loss in the evolution of planarians. *Science* **335**, 461–463 (2012).
38. Ito, D. et al. Pericentrin-mediated SAS-6 recruitment promotes centriole assembly. *eLife* **8**, e41418 (2019).
39. Kubo, A., Sasaki, H., Yuba-Kubo, A., Tsukita, S. & Shiina, N. Centriolar satellites: molecular characterization, ATP-dependent movement toward centrioles and possible involvement in ciliogenesis. *J. Cell Biol.* **147**, 969–979 (1999).
40. Gheiratmand, L. et al. Spatial and proteomic profiling reveals centrosome-independent features of centriolar satellites. *EMBO J.* **38**, e101109 (2019).
41. Quarantotti, V. et al. Centriolar satellites are acentriolar assemblies of centrosomal proteins. *EMBO J.* **38**, e101082 (2019).
42. Kodani, A. et al. Centriolar satellites assemble centrosomal microcephaly proteins to recruit CDK2 and promote centriole duplication. eLife **4**, e07519 (2015).
43. Firat-Karalar, E. N., Rauniyar, N., Yates, J. R. 3rd & Stearns, T. Proximity interactions among centrosome components identify regulators of centriole duplication. *Curr. Biol.* **24**, 664–670 (2014).

Methods

Mouse models. The mice were housed and cared for in an AAALAC-accredited facility and the experiments were conducted in accordance with protocols approved by the Institute Animal Care and Use Committee (for A.J.H.) or in conformity with French and European Union regulations and the recommendations of the local ethics committee (Comité d'éthique en expérimentation animale n°005; for AM). The study is compliant with all of the relevant ethical regulations regarding animal research.

Deup1$^{-/-}$ *mice. Deup1* heterozygous sperm (*Deup1*$^{tm1.1(KOMP)Vlcg}$) was obtained from the U.C.-Davis Knockout Mouse Phenotyping Consortium (project ID: VG11314). NIH grants to Velocigene at Regeneron Inc (U01HG004085) and the CSD Consortium (U01HG004080) funded the generation of gene-targeted ES cells for 8,500 genes in the KOMP Program and archived and distributed by the KOMP Repository at UC Davis and CHORI (U42RR024244). The mice were rederived at the Transgenic Core Laboratory, Johns Hopkins University School of Medicine, using C57B/L6N mice. These animals were maintained on a congenic C57BL/6N background. The following primers pairs were used for genotyping: Mut For, 5′-acttgctttaaaaaacctcccaca-3′ and Mut Rev, 5′-ggaagtagactaacgtggagcaagc-3′; WT For, 5′-tagggcactgttgggtatattgg-3′ and WT Rev, 5′-ccacacatttctgcttctcc-3′. Embryos and adults from both genders were included in our analysis.

Cep63$^{T/T}$ *mice. Cep63*$^{T/T}$ mice were obtained from the laboratory of T. Stracker (Institute for Research in Biomedicine Barcelona). The generation of these *Cep63* gene-trapped mice was described previously[28,29]. The *Cep63*$^{T/T}$ mice were backcrossed for two generations onto a C57Bl/6N strain. The following primers were used for genotyping: Cep63-5P2, 5′-gtaggaccaggccttagcgttag-3′; Cep63-3P1a, 5′-taagtgtaaaagccgggcgtggt-3′ and MutR (B32), 5′-caaggcgattaagttgggtaacg-3′.

CENT2–GFP mice. CENT2–GFP mice (CB6-Tg(CAG-EGFP/CETN2)3-4Jgg/J) were obtained from The Jackson Laboratory[26]. These animals were maintained on a C57Bl/6J background. Experiments were performed on cells from homozygous or heterozygous *CENT2–GFP* mice.

Double transgenic CENT2–GFP; Deup1$^{-/-}$ *mice.* Homozygous *CENT2–GFP* mice were crossed with *Deup1*$^{-/-}$ mice to generate *CENT2–GFP*$^{+/-}$; *Deup*$^{+/-}$ mice. These double heterozygous mice were then crossed to produce *Deup1*$^{-/-}$ mice (identified through genotyping) positive for CENT2–GFP (either *CENT2–GFP*$^{+/-}$ or *CENT2–GFP* $^{+/+}$; identified using a fluorescence binocular).

Cell culture. *Primary cells.* The mTEC cultures were harvested and grown as previously described[24]. Briefly, tracheas were harvested from mice that were between 3 weeks and 12 months old. The tracheas were then incubated overnight in Pronase (Roche) at 4 °C. The tracheal cells were dissociated by enzymatic and mechanical digestion the following day. The cells were plated onto 0.4-µm Falcon transwell membranes (Transwell, Corning). Once the cells were confluent (around proliferation day 5), the medium from the apical chamber was removed and the basal medium was replaced with low serum (NuSerum) medium. This time point is considered air–liquid interface day 0. The cells were then allowed to differentiate until needed for analysis (air–liquid interface days 3 or 5).

For the mouse ependymal cell cultures, the brains were dissected from P0–P2 mice, dissociated and cultured as previously described[25]. Briefly, the mice were killed by decapitation. The brains were dissected in Hank's solution (10% HBSS, 5% HEPES, 5% sodium bicarbonate and 1% penicillin/streptomycin (P/S) in pure water) and the telencephalon were manually cut into pieces, followed by enzymatic digestion (DMEM GlutaMAX, 3% papain (Worthington 3126), 1.5% 10 mg. ml^{-1} DNAse and 2.4% 12 mg.ml^{-1} cystein) for 45 min at 37 °C in a humidified 5% CO_2 incubator. The digestion was stopped by the addition of a solution of trypsin inhibitors (Leibovitz's L15 medium, 10% 1 mg ml^{-1} ovomucoid and 2% 10 mg ml^{-1} DNAse). The cells were then washed in L15 medium and resuspended in DMEM GlutaMAX supplemented with 10% fetal bovine serum (FBS) and 1% P/S in a poly-L-lysine-coated flask. The ependymal progenitors were allowed to proliferate for 4–5 d, until confluence was reached, before being incubated overnight with shaking (250 r.p.m.). The pure confluent astroglial monolayers were re-plated at a density of 7×10^4 cells cm^{-2} (differentiation day -1) in DMEM GlutaMAX, 10% FBS and 1% P/S on poly-L-lysine-coated coverslides for the immunocytochemistry experiments, Lab-Tek chambered coverglasses (eight-well; Thermo Fisher Scientific) for the time-lapse experiments, four-well glass-bottom slides (Ibidi) for the measurements of the ciliary beating frequency or glass-bottom dishes with imprinted 50-mm relocation grids (Ibidi) for correlative light/electron microscopy and maintained overnight. The medium was then replaced with serum-free DMEM GlutaMAX 1% P/S to trigger ependymal differentiation in vitro (differentiation day 0).

Cell lines. Flp-in TRex-DLD-1 (ref. [44]) and HEK293FT cells were grown in DMEM (Corning) containing 10% FB Essence (VWR Life Science Seradigm) and 100 U ml^{-1} of penicillin and streptomycin. All cells were maintained at 37 °C in 5% CO_2 and atmospheric oxygen.

Centrinone treatment to deplete parent centrioles. Centrinone treatment was carried out as previously described[17]. Briefly, centrinone (MedChemExpress) was added on day 2 of the proliferation phase of ependymal progenitor cultures at a final concentration of 0.6 µM. The centrinone was removed by three washes with PBS at the end of the proliferation phase immediately before trypsinization and re-plating at high confluence for ependymal MCC differentiation (differentiation day -1).

siRNA knockdown. The siRNA transfections were performed at differentiation day -1 on trypsinized cells in suspension using the Jetprime (Polyplus). The ependymal cells (1.3×10^6) were transfected with 100 nM of either ON-TARGETplus non-targeting siRNA (Dharmacon, cat. no. D-001810-01-05) or ON-TARGETplus Deup1 siRNA (Dharmacon, cat. no. L-042708-01-0005) and seeded onto four coverslips. The cells were fixed and analysed 4 d after serum starvation (differentiation day 4).

Cloning and transfection. *Deup1* full-length and exons 8–12. The full-length mouse *Deup1* open reading frame or *Deup1* exons 8–12 were cloned into the pcDNA5/FRT/TO vector. A Myc tag was inserted at the 3′ end of the complimentary DNA sequence. *Deup1* transgenes were inserted into a single genomic locus in the Flp-in TRex-DLD-1 cells using FLP-mediated recombination. DLD-1 cells were seeded in a six-well plate at 2×10^5 cells well^{-1}. The next day, a transfection mixture of 100 µl Opti-MEM (Thermo Fisher Scientific; cat. no. 31985070), 3 µl X-tremeGene HP (Sigma-Aldrich, cat. no. 6366236001), 100 ng pcDNA5 plasmid and 900 ng POG44 (Flp recombinase) was prepared and incubated at room temperature for 30 min and then added drop-wise to each well. Two days later, the cells were selected with 50 µg ml^{-1} hygromycin B (Thermo Fisher, cat. no. 10687010). The HEK293FT cells were transfected using PEI reagent as previously described[44].

Morpholino experiments. For the morpholino validation experiments, morpholino-targetable *Cep63* was PCR amplified from *X. laevis* cDNA and cloned into the PCS2+ vector with a C-terminal EGFP. Morpholino-targetable *Deup1* was produced by annealing two complementary primers consisting of the *Deup1* morpholino sequence and cloned into the PCS2+ vector with a C-terminal EGFP. The plasmids were linearized and mRNA was made from both of these constructs using the mMESSAGE mMACHINE Sp6 transcription kit (Thermo Fisher, AM1340) and purified using an RNA isolation kit (QIAGEN).

Embryo injections. X. laevis embryos were obtained by standard in vitro fertilization protocols approved by the Northwestern University Institutional Animal Care and Use Committee. Morpholinos were designed targeting *Xenopus Deup1* and *Cep63* (Gene Tools, LLC). The *Deup1* morpholino had the sequence 5′-ggctttcagtgtctgtttgcatttc-3′ and the *Cep63* morpholino had the sequence 5′-cattccgttttctcaacacactgca-3′. The embryos were injected with 10–20 ng of morpholino and with Dextran-Cascade Blue (Thermo Fisher, D1976) as a tracer at the two- to four-cell stage. Standard scrambled morpholino controls were used in all morpholino experiments (Gene Tools, LLC). For the morpholino validation experiments, the morpholino-targetable Deup1–GFP or Cep63–GFP RNAs were injected 4× in embryos at the two- to four-cell stage and the corresponding morpholinos were then injected as mosaics in two of the four blastomeres at the four-cell stage with membrane red fluorescent protein or dextran-blue as tracers.

Processing of cells and tissues for immunofluorescence microscopy. *Brains for the ex vivo imaging of ependymal cells.* For the centriole quantification, adult mice were perfused with 1% paraformaldehyde (PFA) and dissected brains were post-fixed overnight in 1% PFA at 4 °C. The following day, the brains were washed 3× in PBS for 1 h at room temperature and then embedded in 3% low-melting-point agarose. The brains were cut coronally into 100 µm sections using a vibratome (Leica Biosystems). The brain sections were stained overnight at 4 °C with primary antibodies diluted in 10% donkey serum (in PBST; 1×PBS and 0.5% Triton X-100). The next day, the sections were washed 3× with PBST at room temperature and then incubated overnight with secondary antibodies and 1 µg ml^{-1} 40,6-diamidino-2-phenylindole (DAPI) diluted in 10% donkey serum at 4 °C. The sections were then washed 3× with PBST at room temperature and mounted onto slides using Fluoromount G mounting media (SouthernBiotech).

To stain the different phases of centriole amplification, lateral brain ventricles from P2–P6 pups were first pre-permeabilized in 0.2% Triton X-100 in BRB medium (80 mM PIPES, 1 mM $MgCl_2$ and 1 mM EGTA) for 2 min before fixation. The tissues were then fixed in methanol for 10 min at −20 °C. The samples were pre-blocked in 1×PBS with 0.2% Triton X-100 and 10% FBS before incubation with the primary and secondary antibodies. The tissues were counterstained with DAPI (10 µg ml^{-1}; Sigma) and mounted in Fluoromount (SouthernBiotech).

mTEC cultures. Membranes were incubated in microtubule stabilization buffer (30% glycerol, 100 mM PIPES, 1 mM EGTA and 1 mM $MgSO_4$) for 60 s, followed by fixation in 4% PFA for 10 min at room temperature. The membranes were washed 3× with PBST (1×PBS and 0.1% Triton X-100) for 5 min each. The membranes were then blocked at room temperature for 1 h. The membranes were cut into

quarters and incubated with primary antibodies diluted in blocking buffer for 1 h at room temperature. Next, the membranes were washed 3× in PBST for 5 min each and incubated for 45 min at room temperature with secondary antibodies diluted in blocking buffer. Finally, the membranes were incubated for with DAPI (10 μg ml^{-1}; Sigma) diluted in PBS 1 min at room temperature and mounted onto slides using ProLong Gold Antifade (Invitrogen).

Ependymal cell cultures. Cells were grown on 12-mm glass coverslips as described above and fixed for 10 min in either 4% PFA at room temperature or 100% ice-cold methanol at −20 °C. The cells were fixed on differentiation day 2–6 for the analysis of centriole amplification and on differentiation day 10 for the analysis of differentiated cells. The samples were pre-blocked in PBS with 0.2% Triton X-100 and 10% FBS before incubation with the primary and secondary antibodies. The cells were counterstained with DAPI (10 μg ml^{-1}; Sigma) and mounted in Fluoromount (SouthernBiotech).

Xenopus. Embryos in the morpholino validation experiment were fixed for 2 h in 3% PFA in PBS, washed in PBST (1×PBS and 0.1% Triton X-100) and then stained with phallodin-647 (Invitrogen). The embryos used for centriole analysis were fixed in 100% ice-cold methanol for 48 h at −20 °C. The embryos were rehydrated in a methanol series, washed in PBST and blocked in 10% heat-inactivated goat serum for 2 h. Mouse anti-centrin (EMD Millipore, cat. no. 04-1624) and rabbit anti-ZO-1 (Invitrogen, cat. no. 61-7300) primary antibodies were used, followed by Cy-2- and Cy-3-conjugated secondary antibodies (Jackson ImmunoResearch Laboratories, Inc.).

Ciliary beat frequency. Cells were seeded onto a four-well glass-bottom slide (Ibidi) and imaged at differentiation day 7 on a 3i Live-cell spinning disk confocal (Zeiss) microscope using a ×32 air objective with ×1.6 magnification. The cells were imaged using wide-field light with a 3-ms exposure time at 330 frames s^{-1} for 10 s. The number of beats per second was measured using previously described methods[45]. Briefly, a 16×16 pixel region of interest containing a single beating cilium was selected and the changes in intensity over time were counted using the ImageJ *z*-axis profile tool. The total number of beats over a 3–5 s interval was measured and used to calculate the average beats s^{-1} for each cell. One to three regions were measured for each cell and used to plot the average beat frequency for each cell.

Cilia-length measurement. The cilia length was measured from the SEM images of MCCs in the mouse trachea. The length was measured using ImageJ software. Three cilia per cell were measured and the average length per cell for each mouse was plotted.

Antibodies. The staining of cells and tissues was performed with the following primary antibodies: goat polyclonal anti-γ-tubulin-555 (ref. [46]; homemade, raised against the peptide CDEYHAATRPDYISWGTQEQ), mouse monoclonal anti-centrin, clone 20H5 (1:3,000; Millipore, 04-1624), rabbit polyclonal anti-CEP164 (1:1,000; EMD Millipore, ABE2621), mouse monoclonal acetylated-α-tubulin (1:1,000; Cell Signaling Technologies, cat. no. 12152), rat polyclonal anti-ZO-1 (1:1,000; Thermo Fisher Scientific, 14-9776-82), rabbit polyclonal anti-DEUP1 no. 1 (1:1,000; homemade, raised against the full-length protein, see below), rabbit anti-DEUP1 (1:2,000; homemade, raised against the peptide TKLKQSRHI)[17], mouse anti-GT335 (1:500; Adipogen, AG-20B-0020-C100), mouse anti-SAS6 (1:750; Santa Cruz, sc-81431), rabbit anti-PCNT (1:2,000; Covance, PRB 432-C) and rabbit anti-CEP63 (1:500; Proteintech, 16268-1-AP). The secondary antibodies were conjugated to Alexa Fluor 488, 555 or 650 (Life Technologies).

Custom-made Deup1 antibodies. The full-length mouse *Deup1* was cloned into a pET-28M bacterial expression vector (EMD Millipore) containing a C-terminal 6-His tag. Recombinant protein was purified from *Escherichia coli* (Bl21^{Rosetta}) cells using Ni-NTA beads (QIAGEN) and 2 mg was used to immunize two rabbits (ProSci Incorporated). The rabbit immune sera were affinity-purified. The purified antibodies were directly conjugated to Alexa Fluor 555 and 650 fluorophores (Thermo Fisher Scientific) for use in immunofluorescence. A rabbit anti-Deup1 (1:2,000) antibody raised against the peptide TKLKQSRHI was previously described[17].

Microscopy. *Immunofluorescence microscopy.* Cells were imaged using a Zeiss LSM700 confocal microscope controlled by ZEN software for centriole counting in mTECs and brain sections. Images were collected using a Zeiss ×63 (1.4 numerical aperture, NA) oil objective at 0.3 μm *z*-sections using Zeiss immersion oil (refractive index N = 1.518).

For centriole counting in cultured ependymal cells and DLD-1 cells, the cells were imaged using a DeltaVision Elite system (GE Healthcare) and a scientific CMOS camera (pco.edge 5.5). The equipment and acquisition parameters were controlled by the SoftWoRx suite (GE Healthcare). Images were collected using an Olympus ×60 (1.42 NA) objective at 0.2 μm *z*-sections using Applied Precision immersion oil (N = 1.516). The cells were imaged using an upright epifluorescence microscope (Zeiss Axio Observer.Z1) controlled by ZEN software for amplification-phase imaging in cultured ependymal cells. Images were collected using a Zeiss apochromat ×63 (1.4 NA) oil objective and a Zeiss Apotome with an H/D grid at 0.24 μm *z*-sections using Zeiss immersion oil (N = 1.518). For the imaging of brain cells in the amplification phase, an inverted LSM 880 Airyscan Zeiss microscope with 440, 515, 560 and 633 laser lines controlled by ZEN software was used. Images were collected using a Zeiss apochromat ×63 (1.4 NA) oil objective at 0.24 μm *z*-sections using Zeiss immersion oil (N = 1.518).

All microscopy on *Xenopus* was performed on a laser-scanning confocal microscope (A1R; Nikon) using a ×60 (1.4 NA) oil plan-apochromat objective lens. The embryos were imaged at room temperature in Fluro-gel (Electron Microscopy Sciences) using the Nikon Elements software. Images were analysed for centriole number and mean fluorescent intensity using ImageJ.

Live-cell imaging. Cultured cells between differentiation days 2 and 6 were filmed using an inverted spinning disk Nikon Ti PFS microscope equipped with ×63 (1.32 NA) and ×100 (1.4 NA oil) immersion objectives, an Evolve EMCCD Camera (Photometrics), diode-pumped solid-state laser (491 nm, 25% intensity, 70 ms exposure), appropriate filter sets for DAPI/FITC/TRITC, a motorized scanning deck and an incubation chamber (37 °C, 5% CO_2 and 80% humidity). Images were acquired using Metamorph Nx at time intervals of 40 min. Image stacks were recorded with a *z*-step of 0.7 μm. The presence or absence of parent centrioles in centrinone-treated cells was monitored using the Cen2–GFP signal at the beginning of centriole amplification.

SEM. The Johns Hopkins microscopy facility performed the SEM. Briefly, tracheas were cut open lengthwise and fixed overnight at 4 °C in a buffer of 2.5% glutaraldehyde, 100 mM sodium cacodylate and 3 mM $MgCl_2$, pH 7.2. Following a rinse in a buffer of 3% sucrose, the samples were post-fixed for 1.5 h on ice in the dark with 2% osmium tetroxide in 100 mM cacodylate buffer containing 3 mM $MgCl_2$. The samples were rinsed in dH_2O and dehydrated through a graded series of ethanol to 90%. Dehydration was continued through 100% ethanol and then passed through a 1:1 solution of ethanol:hexamethyldisiloxazne (Polysciences), followed by pure hexamethyldisiloxazne. The samples were then placed overnight in a desiccator to dry. The tracheal pieces were attached to aluminium stubs via carbon sticky tabs (Pella) and coated with 40 nm of AuPd with a Denton vacuum desk III sputter coater. The stubs were viewed on a Leo 1530 FESEM operating at 1 kV and digital images were captured using SmartSEM version 5.

TEM and CLEM. The CLEM was done as previously described[12]. Briefly, primary CENT2–GFP ependymal progenitors were grown in 0.17-mm-thick glass dishes with imprinted 50-μm relocation grids (Ibidi). At differentiation days 3–6, the cells were fixed with 4% PFA for 10 min and ependymal progenitors undergoing the amplification or growth phase were imaged for CENT2–GFP and DAPI, in PBS, with an upright epifluorescence microscope (Zeiss Axio Observer.Z1). The coordinates of the cells of interest on the relocation grid were recorded. The cells were then processed for TEM. Briefly, the cultured cells were treated with 1% osmium tetroxide, washed and progressively dehydrated. The samples were then incubated in 1% uranyl acetate in 70% methanol before the final dehydration, pre-impregnation with ethanol/epon (2/1, 1/1, 1/2) and impregnation with epon resin. After mounting in epon blocks for 48 h at 60 °C to ensure polymerization, the resin blocks were detached from the glass dish by several baths in liquid nitrogen. Using the grid pattern imprinted in the resin, 50 serial ultra-thin 70-nm sections of the squares of interest were cut using an ultramicrotome (Ultracut EM UC6, Leica) and transferred onto formvar-coated electron microscopy grids (0.4×2 mm slot). The central position of the square of interest and DAPI staining were used to relocate and image the cell of interest using a Philips Technai 12 TEM.

RNA isolation, cDNA synthesis and qPCR. Total RNA was extracted from cells and tissues using TRIzol reagent (Thermo Fisher Scientific) following the manufacturer's protocol. SuperScriptIV reverse transcriptase (Thermo Fisher Scientific) was used for cDNA synthesis. The cDNA was then used for quantitative real-time PCR (Bio-Rad) using SYBR Green qPCR mastermix reagent (Thermo Fisher Scientific). The following primers were used: Deup1 (deleted exons): For, 5′-gccagatgtagacatttcttggcatgg-3′ and Rev: 5′-cccacctcctggccttt-3′; Deup1 (exons 10–12): For, 5′-tacgtcttccagagccagc-3′ and Rev, 5′-caggaagtgctgtgcagc-3′; Deup1 (exons 9–10): For, 5′-gaattaagcaaggctgtggact-3′ and Rev, 5′-ctctggaagacgtatgcccc-3′; Cep63 (exons 6–8): For, 5′-atcagacctacagttctgcc-3′ and Rev, 5′-ctgacttagaatctccttatgctc-3′; Cep63 (exons 13–14): For, 5′-gcaggaggaattaagcagact-3′ and Rev, 5′-ctgtcggaattcctctatttttccag-3′ and GAPDH: For, 5′-aatgtgtccgtcgtggatctga-3′ and Rev, 5′-gatgcctgcttcaccaccttct-3′.

All samples were normalized to GAPDH (ΔC_t). The relative fold change in mRNA expression was quantified using the $2^{-\Delta\Delta C_t}$ method comparing experimental samples to controls. All data were then normalized to the average value of the control samples.

Western blotting. For the immunoblot analyses of protein, cells were lysed in 2×sample buffer (125 mM Tris–HCl, pH 6.8, 20% glycerol, 4% SDS, 0.1% bromophenol blue and 4% β-mercaptoethanol). The samples were then separated by SDS–PAGE, transferred onto a nitrocellulose membrane using a Trans-blot turbo transfer system (Bio-Rad Laboratories) and blocked in 5% milk for 1 h at room temperature. The membranes were incubated for 2 h at room temperature

with primary antibodies diluted in 5% milk, washed 3× with TBST (1×TBS and 1% Tween-20) for 10 min each and then incubated with a horseradish-peroxidase-conjugated secondary antibody diluted in 5% milk. The blots were washed 3× in TBST for 10 min each. The blots were incubated with either SuperSignal west pico PLUS or Femto enhanced chemiluminescent substrate (Thermo Fisher Scientific) for 1 min and imaged using a G:Box (SynGene). The following primary antibodies were used: YL1/2 (rat anti–α-tubulin; 1:3,000; Pierce Antibodies) and rabbit anti-Deup1 no. 2 (1 μg ml^{-1}; custom made). The following secondary antibodies were used: anti-rat or anti-rabbit IgG linked to horseradish peroxidase (Cell Signaling Technologies).

Quantification of centriole number in fixed samples. Regions that contained a high density of MCCs were selected. At least three fields of view were selected per sample and all multiciliated cells within those fields of view were counted until the number of quantified cells across all fields exceeded 30. Cells for which individual centrioles could not be resolved were excluded from our analysis. The centrin or CEP164 foci in each cell were quantified using three-dimensional image stacks and the multipoint tool in ImageJ.

Quantification of centriole number using CENT2–GFP movies. The total number of centrioles was calculated during the disengagement phase when the CENT2–GFP signal was dispersed. The entire volume of the cell was used for the quantification. Image quantification was performed using ImageJ. The presence or absence of parent centrioles in centrinone-treated cells was monitored using the Cen2–GFP signal at the beginning of centriole amplification.

Centriole-length measurement. The centriole length was measured using TEM images. Only centrioles whose axis was parallel to the cut plane were analysed.

Quantification of fluorescence intensity. *SAS6-intensity measurement.* Concentric rings of identical sizes were drawn by hand around the CENT2–GFP-positive parent centrioles and used as regions of interest. An identically sized concentric ring was used for background measurement. Cells for which the SAS6 signal of the two parent centrioles overlapped were excluded. Younger and older parent centrioles were discriminated by staining the primary cilium (GT335^{+}) that is nucleated by the older parent centriole. SAS6 asymmetry was measured as the background-subtracted signal (raw integrated density) of the young parent centriole divided by the background-subtracted signal of the older parent centriole. To calculate the total SAS6 intensity around the parent centrioles, the background-subtracted signals of the older and younger parent centrioles were summed and divided by the background. Image quantification was performed using ImageJ.

PCNT-cloud-intensity measurement. The boundary of the PCNT cloud was determined using a semi-automated segmentation process. Briefly, PCNT staining for each cell was normalized using a Gaussian blur with a radius of three. The automatic 'Otsu' threshold was then applied. The PCNT intensity (raw integrated density) was measured within the resulting mask and divided by the background signal measured in a concentric ring of 4.24 μm^2 in the same cell. Image quantification was performed using ImageJ.

Procentriole localization compared with PCM cloud. The boundary of the PCNT cloud was determined using the semi-automated segmentation process detailed above. The resulting mask was used to identify whether centrioles (marked by SAS6) were located inside or outside the PCNT cloud. Centrioles on the edge of the cloud were considered to be inside. Image quantification was performed using ImageJ.

CEP63-intensity measurement. The boundary of the CEP63 staining was determined using the semi-automated segmentation process detailed above. The CEP63 intensity (raw integrated density) was measured within the resulting mask and divided by the SAS6 intensity within the same mask to normalize for biases that may have arisen from differences in the number of amplified procentrioles in each cell.

DEUP1 variant. The human DEUP1 variant was identified using the gnomAD database (https://gnomad.broadinstitute.org/variant/11-93141472-C-T).

Statistics and reproducibility. Unless otherwise state, the *P* values were calculated using an unpaired two-tailed Welch's *t*-test across the measurements plotted on the graphs (either the averages of at least three independent experiments, or individual measurements when sample size in each experiment was limited). Quantification was semi-automated using a script detailed in the Methods section for the following data: delimitation of the PCNT-cloud border (Fig. 6d and Extended Data Fig. 7b) and quantification of PCNT and CEP63 area and/or intensity (Extended Data Figs. 5b and 7c,d). Quantification of centriole number was performed manually because of the impossibility to have CENT2-GFP bred into all of the genotypes we have analyzed in our study, and because centrin antibodies don't give a sufficient signal-to-noise ratio to automate the segmentation process of centrioles that are small in size and often very close to each other in space. Several levels of redundancy and quality control in our data give us a high degree of confidence in the lack of a substantial difference in centriole number between control and *Deup1*$^{-/-}$ animals. First, the experimenter was blinded to the genotypes when performing quantifications for the initial experiment we performed in the *Deup1*$^{+/+}$ and *Deup1*$^{-/-}$ multiciliated mTECs (Fig. 2a). The data from the following repeats matched what we observed in the initial experiment. Second, quantification of centriole number in the ependymal cells in vivo was performed blinded to genotypes (Fig. 2c and Extended Data Fig. 5h). Third, centriole number was independently quantified on immunostained control and *Deup1*$^{-/-}$ multiciliated ependymal cells in vitro in both the Holland and Meunier laboratories, and the results of these analyses were comparable. Also, the quantification of centriole number in cultured multiciliated ependymal cells performed with fixed imaging in the Holland laboratory (Extended Data Fig. 2a) was very similar to that obtained from a parallel analysis performed in the Meunier laboratory on live cells expressing the CENT2–GFP marker (Fig. 6b). Finally, the analysis of centriole number in *Xenopus* MCCs was performed in the Mitchell laboratory and similar conclusions to what we had observed in mouse MCCs were reached.

Reporting Summary. Further information on research design is available in the Nature Research Reporting Summary linked to this article.

Data availability

Source data for Figs. 1a, 2a,c, 3a, 5a,c,e–g, 6b,d and Extended Data Figs. 1b,c, 2a,c,d, 3a–c,e,f, 5a–d,f,h, 6a,c, 7b–d have been provided online. All other data supporting the findings of this study are available from the corresponding authors on reasonable request.

References

44. Moyer, T. C., Clutario, K. M., Lambrus, B. G., Daggubati, V. & Holland, A. J. Binding of STIL to Plk4 activates kinase activity to promote centriole assembly. *J. Cell Biol.* **209**, 863–878 (2015).
45. Mahuzier, A. et al. Ependymal cilia beating induces an actin network to protect centrioles against shear stress. *Nat. Commun.* **9**, 2279 (2018).
46. Levine, M. S. et al. Centrosome amplification is sufficient to promote spontaneous tumorigenesis in mammals. *Dev. Cell* **40**, 313–322 (2017).

Acknowledgements

We thank all of the members of the Spassky laboratory for their comments and discussions, M. Legendre for identifying the *DEUP1* mutation on the gnomAD control database, K. Oegema and A.K. Shiau (Ludwig Institute for Cancer Research) for sharing centrinone, A.-K. Konate and R. Nagalingum for administrative support and the IBENS Animal Facility for animal care. We thank the IBENS Imaging Facility, with grants from Région Ile-de-France (NERF 2011-45), Fondation pour la Recherche Médicale (FRM; DGE 20111123023), and Fédération pour la Recherche sur le Cerveau–Rotary International France (2011). We thank Y. Wang of the Nathans laboratory for technical assistance. The authors would like to thank the Genome Aggregation Database (gnomAD) and the groups that provided the exome and genome variant data to this resource. We are grateful to J. Nathans, A. Rosen and the Johns Hopkins Institute for Basic Biomedical Sciences for providing research support to A.J.H. This work was supported by grants from the National Institutes of Health (R01GM114119 and R01GM133897) and an American Cancer Society Scholar (RSG-16-156-01-CCG) to A.J.H., National Institutes of Health (R01GM089970) to B.M., Agence Nationale de la Recherche (ANR) Investissements d'Avenir (ANR-10-LABX-54 MEMO LIFE and ANR-11-IDEX-0001-02 PSL Research University) to IBENS. The Spassky laboratory is supported by INSERM, CNRS, EcoleNormale Supérieure (ENS), FRM (EquipeFRM grant 20140329547), a European Research Council (ERC Consolidator grant 647466) to N.S. and ANR (ANRJC JC-15- CE13-0005-01) to A.M.

Author contributions

O.M. and M.S.L. designed, performed and analysed the majority of the experiments, with O.M. performing and analysing the live imaging, super-resolution microscopy and CLEM, and M.S.L. generating and validating the *Deup1*$^{-/-}$ and *Deup1*$^{-/-}$; *Cep63*$^{T/T}$ mice, quantifying the basal body number in all of the genotypes and performing the siRNA experiments. G.M.L quantified the cilia beat frequency and cilia length. V.G. and A.K. assisted with the image quantification and P.R. performed the electron microscopy sample preparation. E.B. and B.J.M. performed and analysed the *Xenopus* multiciliated cell data. N.S., A.M. and A.J.H. analysed the data. A.J.H and A.M. conceived and co-supervised the study. A.J.H., A.M., O.M. and M.S.L. co-wrote the manuscript.

Competing interests

The authors declare no competing interests.

Additional information

Extended data is available for this paper at https://doi.org/10.1038/s41556-019-0427-x.

Supplementary information is available for this paper at https://doi.org/10.1038/s41556-019-0427-x.

Correspondence and requests for materials should be addressed to A.M. or A.J.H.

Reprints and permissions information is available at www.nature.com/reprints.

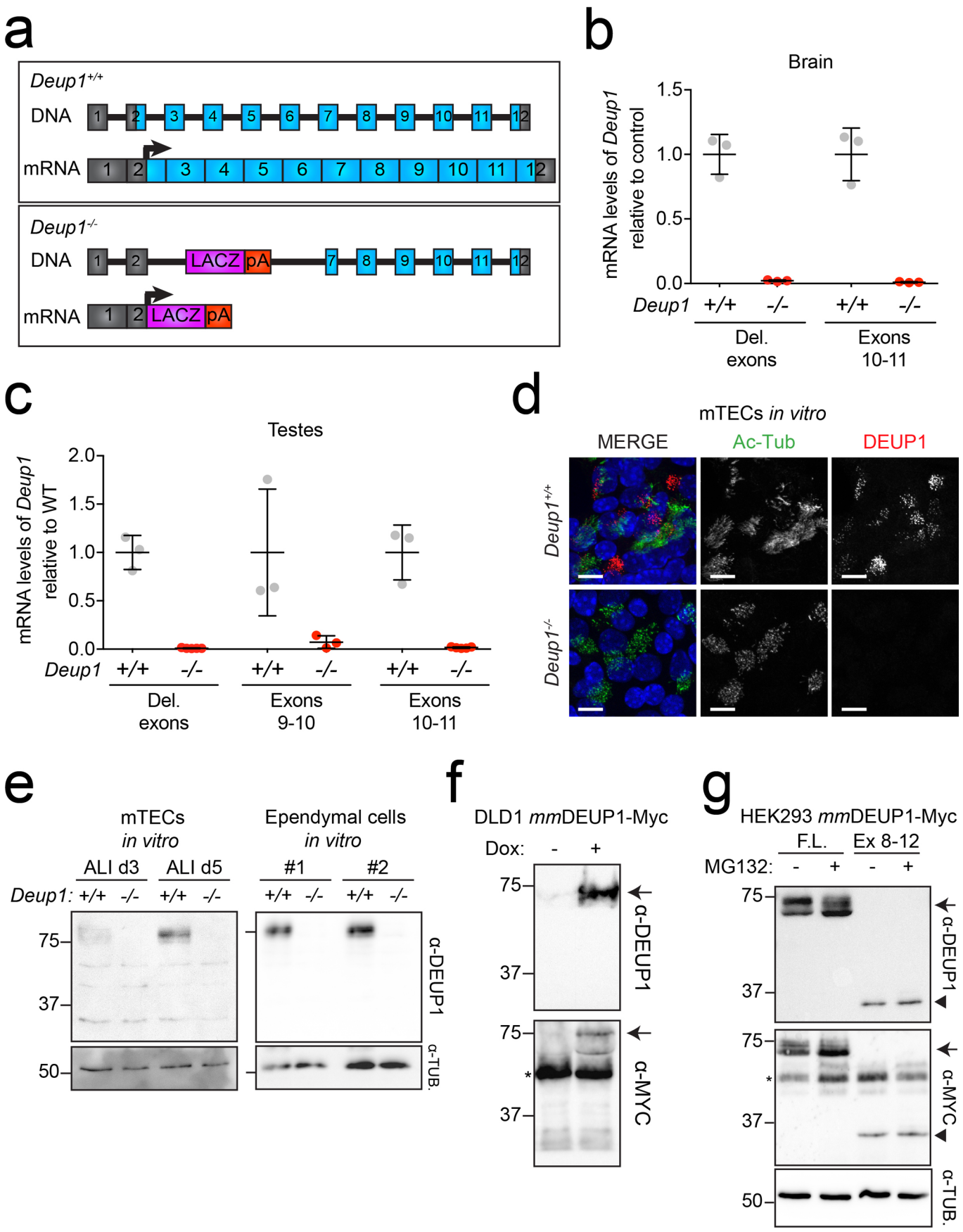

Extended Data Fig. 1 | See next page for caption.

Extended Data Fig. 1 | *Deup1*$^{-/-}$ mice lack *Deup1* mRNA and detectable protein. a, A Deup1 knockout was generated by replacing a region from within exon 2 to within exon 7 of the *Deup1* gene with a LacZ reporter followed by a polyA sequence. (top) Schematic representation of the *Deup1* gene and (bottom) mRNA structure in *Deup1*$^{+/+}$ and *Deup1*$^{-/-}$ mice. **b**, RT-qPCR analysis of *Deup1* mRNA levels in postnatal day 5 brain tissue. Deleted (Del.) exons denote primers designed to amplify exons 2–3 that are deleted in *Deup1*$^{-/-}$ mice. The average of *Deup1*$^{+/+}$ samples was normalized to 1. $n = 3$ mice/genotype. Bars represent mean ± s.d. **c**, RT-qPCR analysis of testes in 2–5-month-old mice using 3 different primer sets. The average of *Deup1*$^{+/+}$ samples was normalized to 1. $n \geq 3$ mice/genotype. Bars represent mean ± s.d. **d**, Immunofluorescence images of mTECs at air–liquid interface (ALI) day 4. Scale bars represent 10 μm. **e**, Western blot of lysates from mTECs at ALI day 3 and 5, and two different ependymal cell cultures differentiated for 8 days. Membranes were probed with antibodies against DEUP1 and α-tubulin was used as a loading control. Full blot shown in Source Data. **f**, Immunoblot of DLD-1 cells expressing doxycycline (dox) inducible *mm*DEUP1-Myc transgene. Membranes were probed with antibodies against DEUP1 or Myc. Arrow denotes the *mm*DEUP1-Myc protein and the asterisk shows endogenous Myc. Full blot shown in Source Data. **g**, Immunoblot of HEK293 cells expressing either full-length (F.L.) or exons 8–12 (Ex 8–12) of *mm*DEUP1 in the presence or absence of the proteasome inhibitor, MG132. MG132 was used to enable the detection of unstable protein fragments. Membranes were probed with antibodies against DEUP1 or Myc. α-tubulin was used as a loading control. Arrow denotes the full-length *mm*DEUP1-Myc protein, arrowhead denotes the exon 8–12 *mm*DEUP1-Myc protein and the asterisk shows endogenous Myc. Full blot shown in Source Data.

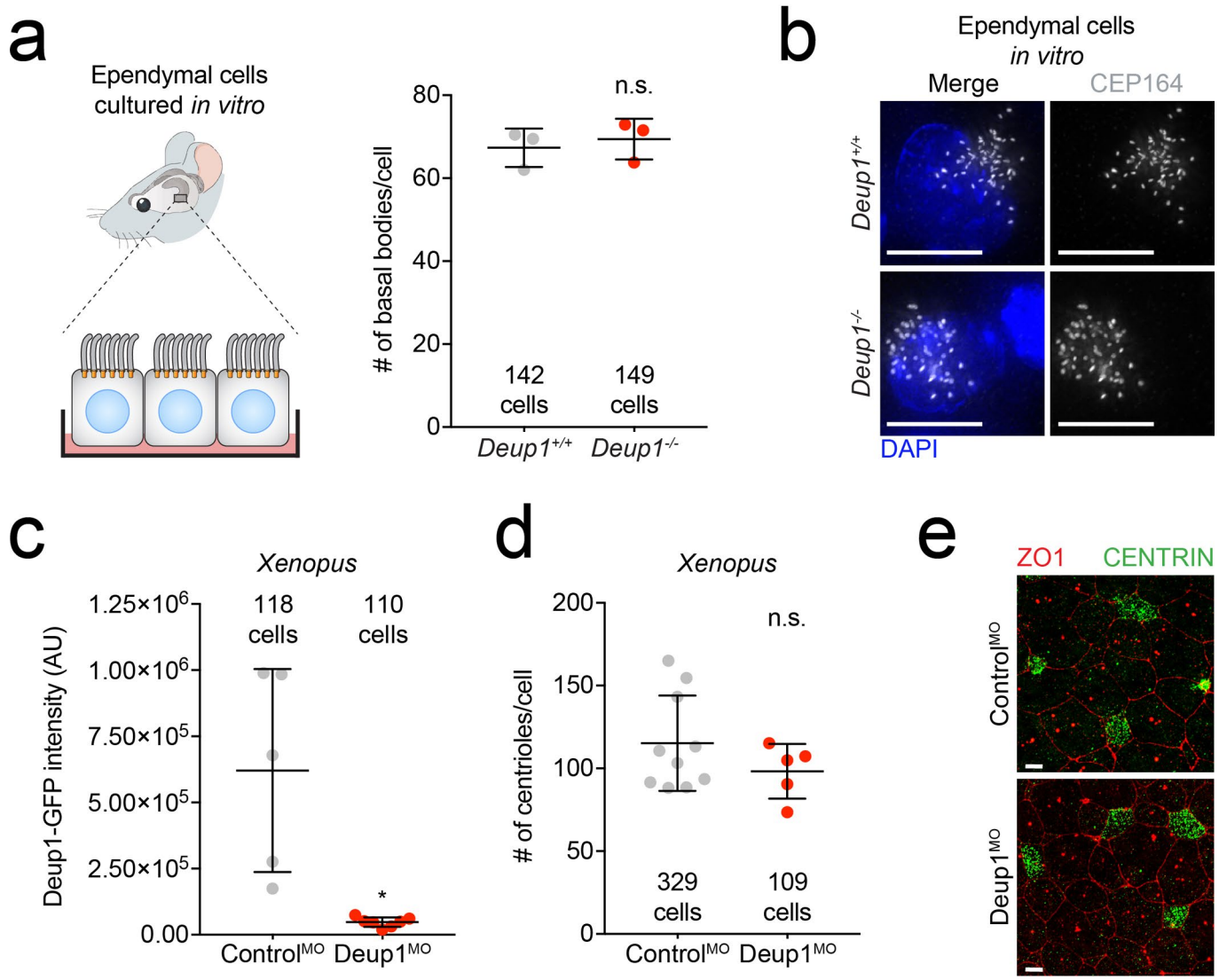

Extended Data Fig. 2 | DEUP1 is not required for centriole amplification. a, Quantification of CEP164 foci which marks the mature basal bodies in control or *Deup1*$^{-/-}$ ependymal cells. The total number of cells analysed per genotype is indicated. $n = 3$ mice/genotype. *P* values, unpaired, two-tailed, Welch's t-test. n.s. = not statistically significant ($p > 0.05$). Bars represent mean ± s.d. **b**, Representative images of mature centrioles in *Deup1*$^{+/+}$ or *Deup1*$^{-/-}$ ependymal cells stained with an antibody against CEP164. Scale bars represent 10 µm. **c**, Quantification of Deup1-GFP intensity in control or Deup1 morpholino-treated *Xenopus* epithelial cells. Note, the Deup1 morpholino oligonucleotide efficiently silenced expression of an mRNA encoding a morpholino-targetable fragment of Deup1 fused to GFP in *Xenopus* MCCs. $n \geq 5$ embryos per genotype. The total number of cells analysed per condition is indicated. *P* values, unpaired, two-tailed, Welch's t-test. * = $p \leq 0.05$. Bars represent mean ± s.d. **d**, Quantification of centriole number in control or Deup1 morpholino-treated *Xenopus* epithelial cells. Points represent the average number of centrioles per embryo. $n \geq 5$ embryos per genotype. The total number of cells analysed per condition is indicated. *P* values, unpaired, two-tailed, Welch's t-test. n.s. = not statistically significant ($p > 0.05$). Bars represent mean ± s.d. **e**, Representative immunofluorescence images from control or Deup1 morpholino-treated *Xenopus* epithelial cells stained with tight junction marker, ZO-1, and centriole marker, Centrin. Scale bars represent 10 µm.

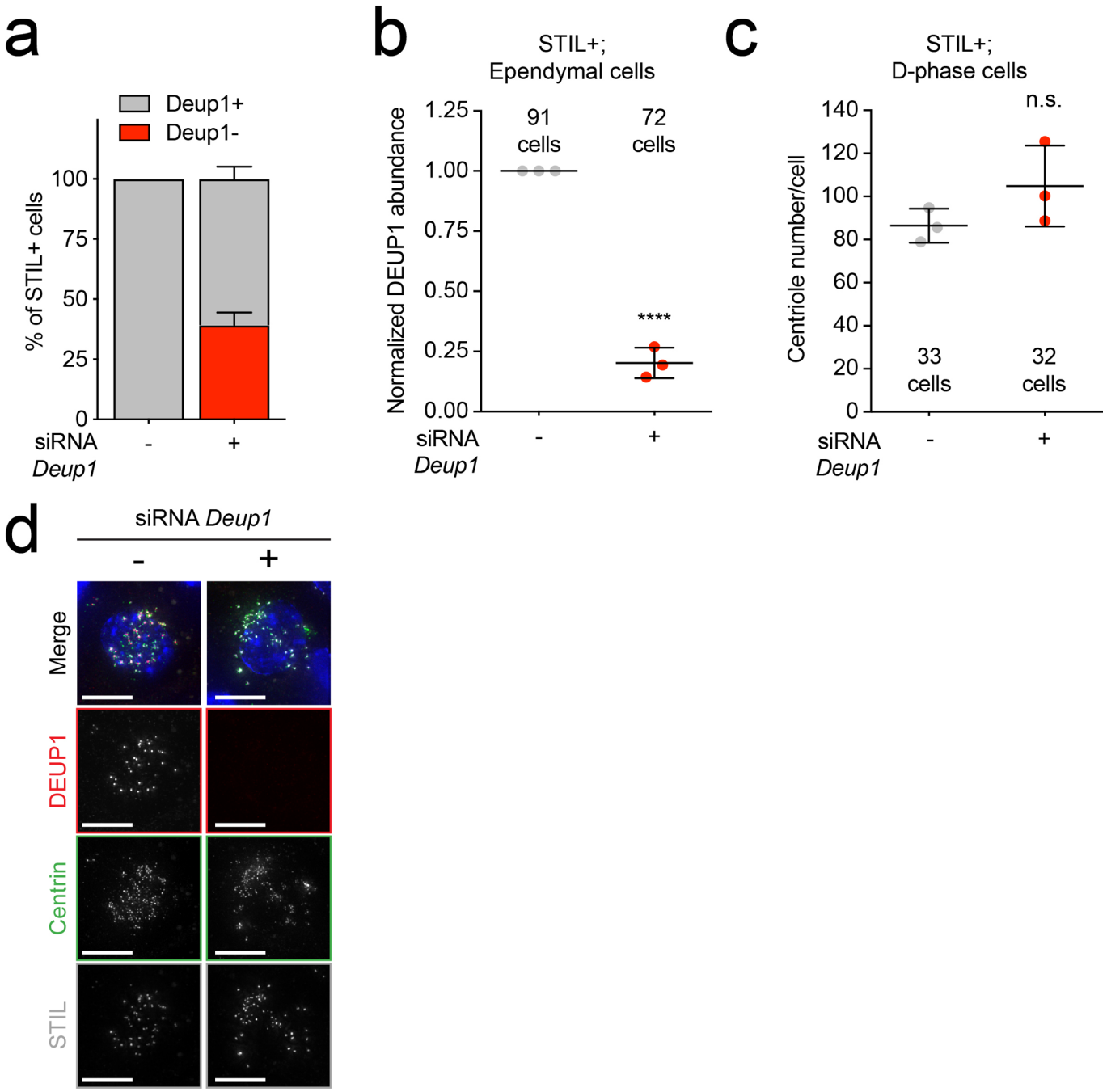

Extended Data Fig. 3 | *Deup1* siRNA does not suppress centriole amplification in MCCs. a, Quantification of control or *Deup1* siRNA-treated cells undergoing centriole amplification that contained (DEUP1+) or lacked (DEUP1-) DEUP1 foci. To identify cells in the process of centriole amplification we immunostained for STIL, which localizes to immature procentrioles but is absent from mature basal bodies. $n = 3$ cultures/genotype. **b**, Quantification of the intensity of DEUP1 signal in STIL+/DEUP1+ controls or STIL+/DEUP1- siRNA-treated cells. $n = 3$ cultures/genotype. The average DEUP1 intensity for the control siRNA sample was normalized to 1 for each experiment. *P* values, one sample t-test compared to a mean of 1. **** = $p \leq 0.0001$. **c**, Quantification of centriole number in control and *Deup1* siRNA-treated cells. Only STIL+ cells were quantified so that DEUP1 depletion could be monitored, and only cells depleted for DEUP1 (assessed by immunostaining) in the siRNA condition were quantified. $n = 3$ cultures/genotype. *P* values, unpaired, two-tailed, Welch's t-test. n.s. = not statistically significant ($p > 0.05$). **d**, Representative images of control ependymal cells and cells with siRNA-mediated depletion of DEUP1 undergoing centriole amplification. Scale bars represent 10 µm.

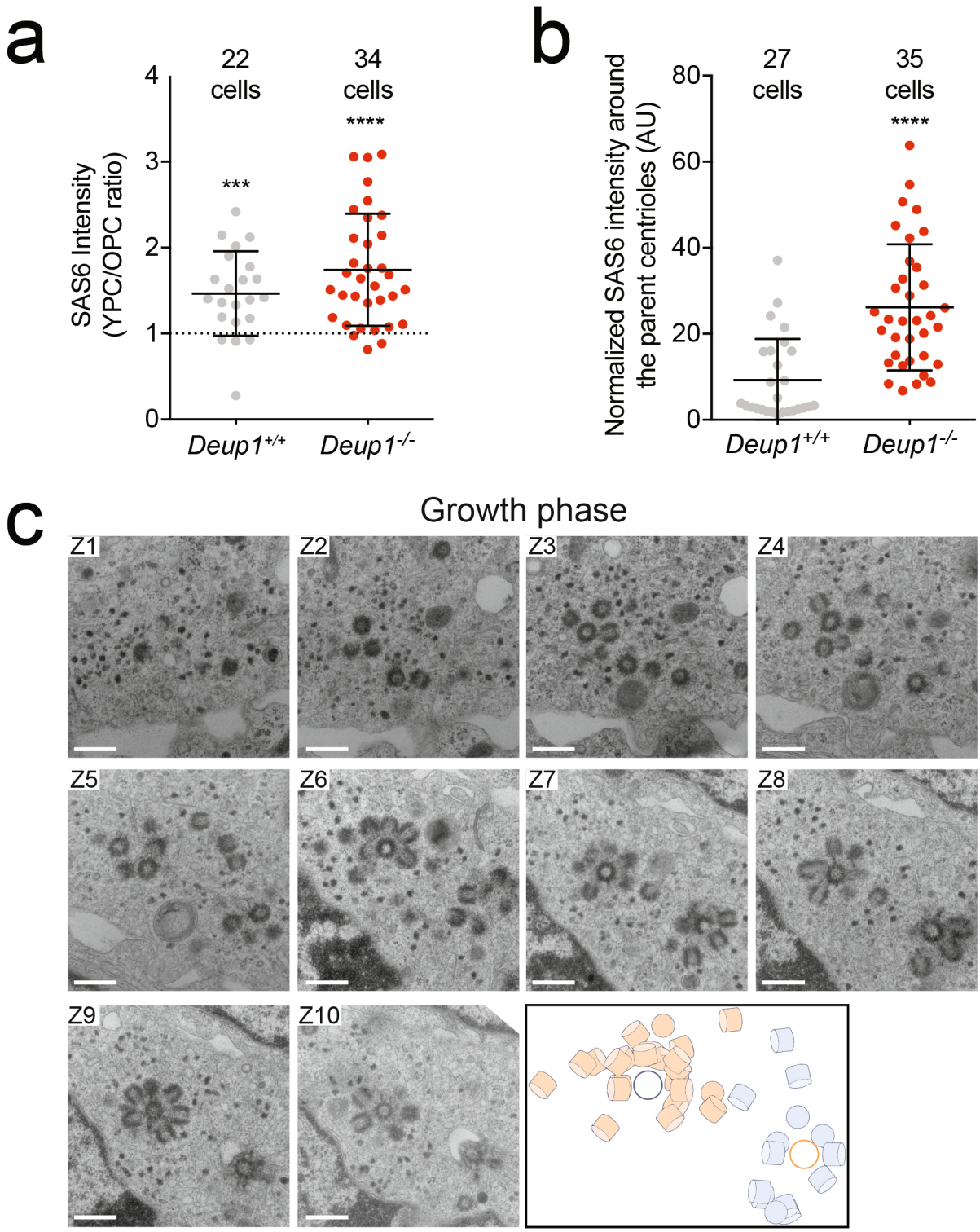

Extended Data Fig. 4 | Procentrioles form in the vicinity of parent centrioles in cells that lack deuterosomes. a, Quantification of the ratio of SAS6 intensity at the younger parent centriole (YPC) compared to the older parent centriole (OPC) in ependymal cells in vivo (P2–P6) during A-phase. GT335 staining was used to mark the cilium that forms from the older parent centriole. $n = 3$ mice/genotype. *P* values, one sample t-test compared to the value of 1, which represents identical SAS6 intensity levels at the YPC and OPC. *** = $p \leq 0.001$, **** = $p \leq 0.0001$. **b**, Quantification of SAS6 intensity on parent centrioles in *Deup1*$^{+/+}$ and *Deup1*$^{-/-}$ ependymal cells in amplification phase in vivo (P2–P6). The SAS6 signal associated with the two parent centrioles was summed together and normalized to background SAS6 staining of the same cell. $n = 3$ mice/genotype. *P* values, unpaired, two-tailed, Welch's t-test. **** = $p \leq 0.0001$. All bars represent mean ± s.d. **c**, Serial EM images of a *Deup1*$^{-/-}$ ependymal cell in the growth phase from basal (Z1) to apical (Z10). Note the important centriole amplification on, and in the vicinity of, the parental centrioles. Bottom right shows a schematic representation of the relative position of procentrioles formed by the parent centrioles. Scale bar represents 500 nm.

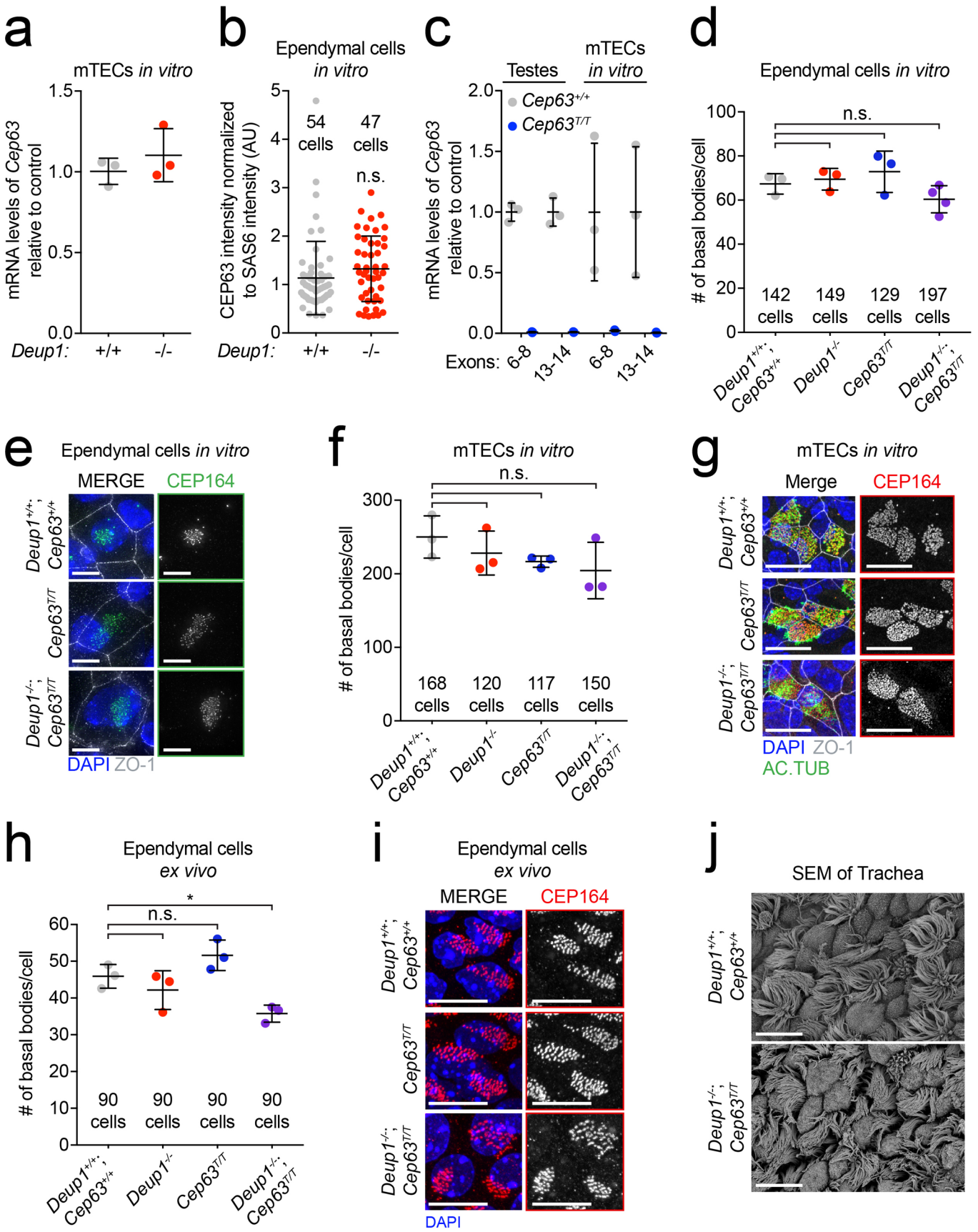

Extended Data Fig. 5 | See next page for caption.

Extended Data Fig. 5 | CEP63 modestly affects centriole amplification in *Deup1*$^{-/-}$ MCCs. a, RT-qPCR analysis of *Cep63* mRNA levels in *Deup1*$^{+/+}$ and *Deup1*$^{-/-}$ mTECs. $n=3$ cultures/genotype. The average of *Deup1*$^{+/+}$ samples was normalized to 1. **b**, Quantification of CEP63 protein levels in ependymal cells in the amplification phase by immunostaining. To account for differences in the number of procentrioles present in each cell, CEP63 intensity levels were normalized to the intensity of the procentriole marker SAS6. $n=3$ cultures/genotype. **c**, RT-qPCR analysis of *Cep63* mRNA levels in testes and mTECs from *Cep63*$^{+/+}$ and *Cep63*$^{T/T}$ mice using two different primer sets. The average of *Cep63*$^{+/+}$ samples was normalized to 1. $n=3$ mice or cultures/genotype. **d**, Quantification of CEP164 foci which marks basal bodies in cultured mature ependymal cells. Data from *Deup1*$^{+/+}$ and *Deup1*$^{-/-}$ cultures are from Extended Data 2a and shown for comparison. $n=3$ cultures/genotype. **e**, Representative images of mature basal bodies using an antibody against CEP164 in mature ependymal cells in vitro. **f**, Quantification of CEP164 foci in mature mTECs. Data from *Deup1*$^{+/+}$ and *Deup1*$^{-/-}$ cultures are from Fig. 2a and shown for comparison. $n=3$ cultures/genotype. **g**, Representative images from mature mTECs. DAPI marks the nuclei, acetylated-tubulin (AcTub) marks cilia, ZO-1 marks tight junctions and CEP164 stains basal bodies. **h**, Quantification of the basal body marker CEP164 foci in adult-brain sections. Data from *Deup1*$^{+/+}$ and *Deup1*$^{-/-}$ mice are from Fig. 2c and shown for comparison. $n=3$ mice/genotype. **i**, Representative images of ependymal cells in adult-brain sections. DAPI marks the nuclei, ZO-1 marks tight junctions and CEP164 stains basal bodies. **j**, Scanning electron micrographs of trachea from control or *Deup1*$^{-/-}$; *Cep63*$^{T/T}$ adult mice. All scale bars represent 10 μm. All bars represent mean ± s.d. All *P* values are from unpaired, two-tailed, Welch's t-test. n.s. = not statistically significant ($p > 0.05$), * = $p \leq 0.05$.

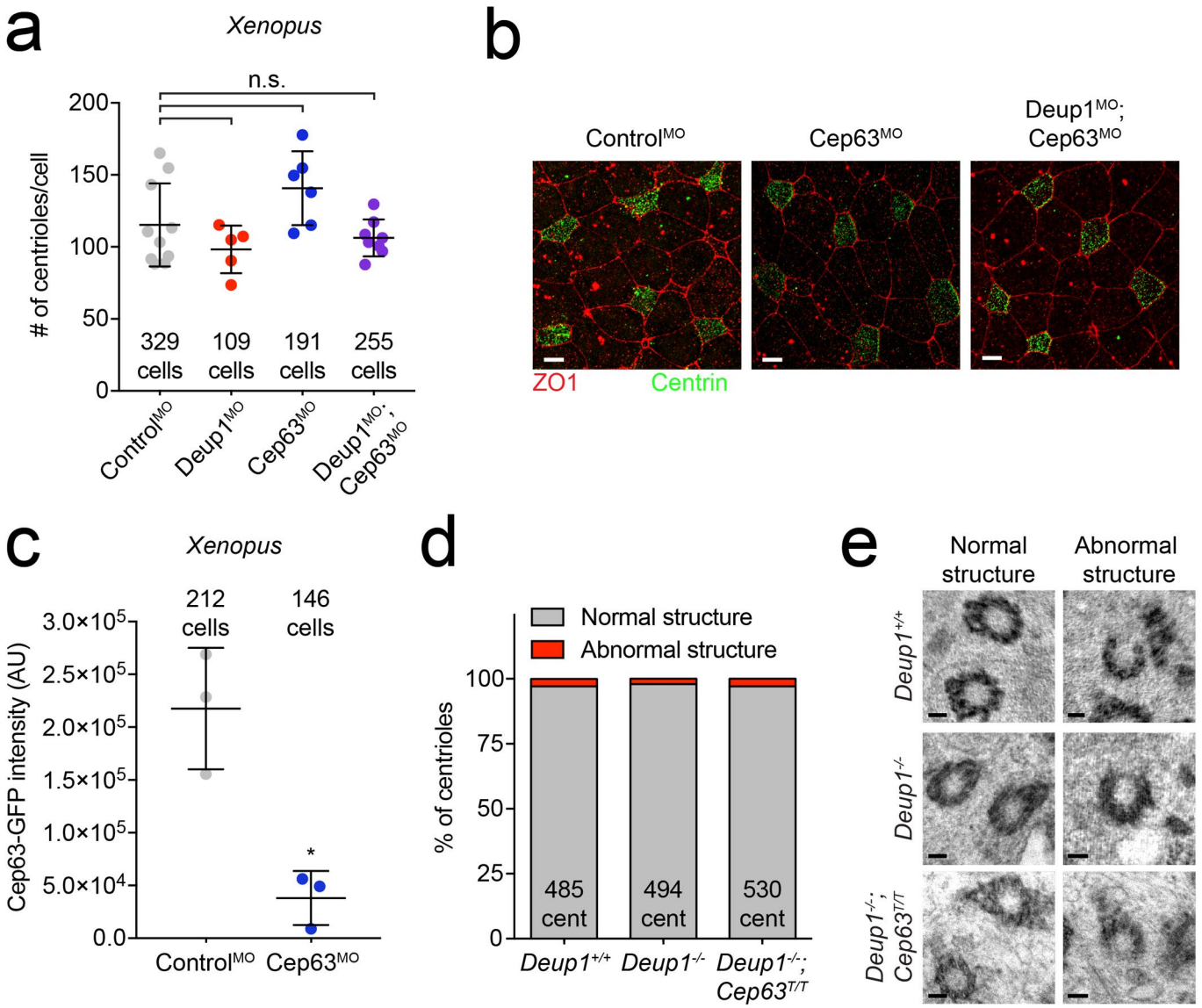

Extended Data Fig. 6 | Deup1 and Cep63 are dispensable for centriole amplification in *Xenopus*. **a**, Quantification of centriole number in *Xenopus* epithelial cells treated with Cep63 or Deup1 and Cep63 morpholinos. Data from control and Deup1 morpholinos are from Extended Data 2d and shown for comparison. Points represent the average number of centrioles per cell in one embryo. $n \geq 5$ embryos/genotype. The total number of cells analysed per condition is indicated. *P* values, unpaired, two-tailed, Welch's t-test. n.s. = not statistically significant ($p > 0.05$). Bars represent mean + s.d. **b**, Representative immunofluorescence images from control, Cep63 or Deup1 and Cep63 morpholino-treated *Xenopus* epithelial cells stained with tight junction marker, ZO-1, and centriole marker, Centrin. Scale bars represent 10 µm. **c**, Quantification of Cep63-GFP intensity in control and Cep63 morpholino-treated *Xenopus* epithelial cells. Note, the Cep63 morpholino oligonucleotide efficiently silenced expression of an mRNA encoding a morpholino-targetable Cep63 fused to GFP in *Xenopus* MCCs. $n = 3$ embryos/genotype. The total number of cells analysed per condition is indicated. *P* values, unpaired, two-tailed, Welch's t-test. * = $p \leq 0.05$. Bars represent mean + s.d. **d**, Quantification of the percent of centrioles with normal or abnormal structure in *Deup1*$^{+/+}$, *Deup1*$^{-/-}$ and *Deup1*$^{-/-}$; *Cep63*$^{T/T}$ cultured ependymal cells. $n > 30$ cells/genotype. The total number of centrioles analysed per genotype is indicated. **e**, Representative TEM images of normal and abnormal centrioles in *Deup1*$^{+/+}$, *Deup1*$^{-/-}$ and *Deup1*$^{-/-}$; *Cep63*$^{T/T}$ cultured ependymal cells. Scale bar represents 100 nm.

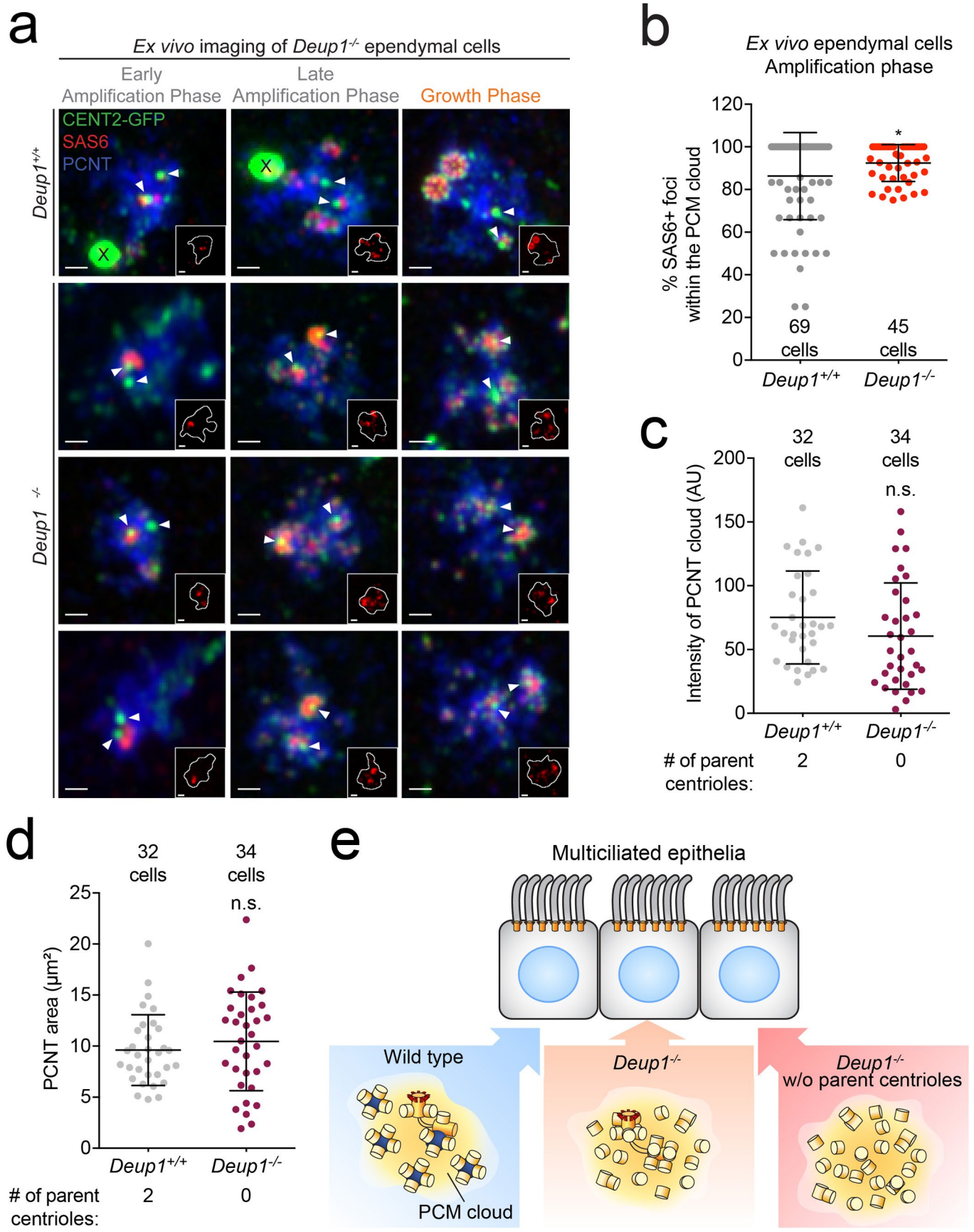

Extended Data Fig. 7 | See next page for caption.

Extended Data Fig. 7 | Procentrioles are amplified within a cloud of PCNT in both *Deup1*$^{+/+}$ and *Deup1*$^{-/-}$ cells with or without parent centrioles. **a**, Immunofluorescence images of CENT2-GFP-expressing *Deup1*$^{+/+}$ and *Deup1*$^{-/-}$ ependymal cells. Brain sections were stained with antibodies against the procentriole protein SAS6 and pericentriolar material protein PCNT. X marks CENT2-GFP aggregates. Arrowheads point to parent centrioles. Insets show the same images with only the SAS6 staining and the PCNT cloud border generated through the semi-automatic segmentation process. Scale bars represent 1 μm. **b**, Quantification of the percent of SAS6^{+} foci observed within the PCNT cloud in *Deup1*$^{+/+}$ and *Deup1*$^{-/-}$ ependymal cells during the amplification phase in vivo. $n = 3$ mice/genotype. Each point represents a single cell. The total number of cells analysed per genotype is indicated. *P* values, unpaired, two-tailed, Welch's t-test. * = $p \leq 0.05$. Bars represent mean ± s.d. **c**, Quantification of the intensity of the PCNT cloud in *Deup1*$^{+/+}$ ependymal cells with 2 parent centrioles and in *Deup1*$^{-/-}$ ependymal cells with 0 parent centrioles during the amplification phase in vitro. $n = 3$ cultures/genotype. The total number of cells analysed per genotype is indicated. *P* values, unpaired, two-tailed, Welch's t-test. n.s. = not statistically significant ($p > 0.05$). Bars represent mean ± s.d. **d**, Quantification of the area of the PCNT cloud in *Deup1*$^{+/+}$ ependymal cells with 2 parent centrioles and in *Deup1*$^{-/-}$ ependymal cells with 0 parent centrioles during the amplification phase in vitro. $n = 3$ cultures/genotype. The total number of cells analysed per genotype is indicated. *P* values, unpaired, two-tailed, Welch's t-test. n.s. = not statistically significant ($p > 0.05$). Bars represent mean ± s.d. **e**, Model of centriole amplification in MCCs. (Blue) Wild type cells amplify centrioles on the surface of deuterosomes and the parent centrioles. (Orange) *Deup1* knockout cells achieve the correct number of centrioles through the massive production of centrioles on the surface and in the vicinity of parent centrioles. (Red) MCCs that lack parent centrioles and deuterosomes amplify the correct number of centrioles within the confines of a PCM cloud.

nature research

Corresponding author(s): Andrew Holland
Alice Meunier

Last updated by author(s): 08.23.19

Reporting Summary

Nature Research wishes to improve the reproducibility of the work that we publish. This form provides structure for consistency and transparency in reporting. For further information on Nature Research policies, see Authors & Referees and the Editorial Policy Checklist.

Statistics

For all statistical analyses, confirm that the following items are present in the figure legend, table legend, main text, or Methods section.

n/a	Confirmed	
☐	☒	The exact sample size (*n*) for each experimental group/condition, given as a discrete number and unit of measurement
☐	☒	A statement on whether measurements were taken from distinct samples or whether the same sample was measured repeatedly
☐	☒	The statistical test(s) used AND whether they are one- or two-sided *Only common tests should be described solely by name; describe more complex techniques in the Methods section.*
☒	☐	A description of all covariates tested
☒	☐	A description of any assumptions or corrections, such as tests of normality and adjustment for multiple comparisons
☐	☒	A full description of the statistical parameters including central tendency (e.g. means) or other basic estimates (e.g. regression coefficient) AND variation (e.g. standard deviation) or associated estimates of uncertainty (e.g. confidence intervals)
☐	☒	For null hypothesis testing, the test statistic (e.g. *F*, *t*, *r*) with confidence intervals, effect sizes, degrees of freedom and *P* value noted *Give P values as exact values whenever suitable.*
☒	☐	For Bayesian analysis, information on the choice of priors and Markov chain Monte Carlo settings
☒	☐	For hierarchical and complex designs, identification of the appropriate level for tests and full reporting of outcomes
☒	☐	Estimates of effect sizes (e.g. Cohen's *d*, Pearson's *r*), indicating how they were calculated

Our web collection on statistics for biologists contains articles on many of the points above.

Software and code

Policy information about availability of computer code

Data collection	N/A
Data analysis	GraphPad Prism software was used to plot data and perform most statistical tests, otherwise statistics were performed in Microsoft Excel. Image analysis and quantification was performed in FIJI.

For manuscripts utilizing custom algorithms or software that are central to the research but not yet described in published literature, software must be made available to editors/reviewers. We strongly encourage code deposition in a community repository (e.g. GitHub). See the Nature Research guidelines for submitting code & software for further information.

Data

Policy information about availability of data

All manuscripts must include a data availability statement. This statement should provide the following information, where applicable:

- Accession codes, unique identifiers, or web links for publicly available datasets
- A list of figures that have associated raw data
- A description of any restrictions on data availability

The data that support the findings of this study are available from the corresponding authors upon reasonable request.

Field-specific reporting

Please select the one below that is the best fit for your research. If you are not sure, read the appropriate sections before making your selection.

☒ Life sciences ☐ Behavioural & social sciences ☐ Ecological, evolutionary & environmental sciences

Life sciences study design

All studies must disclose on these points even when the disclosure is negative.

Sample size	Three mice per group were used in each experiment. Sample size was determined to be adequate based on the magnitude and consistency of measurable differences between groups. At least three mice per group were used in each experiment, with the exception of the experiment in Figure 6d.
Data exclusions	No data were excluded
Replication	Each experiment presented in the paper was repeated in multiple times and/or across multiple animals. Replicate experiments were successful. The precise number of repeats are given in the figure legend.
Randomization	We did not use randomization to assign animals to experimental groups. Mice analyzed were litter mates and sex-matched whenever possible.
Blinding	Investigators were not blinded to mouse genotypes during most experiments. Data reported for mouse experiments are not subjective but rather based on quantitative analysis of centriole number/structure. Analysis of the data in the following figures were performed blinded: Figure 2a,Figure 5g and Supplementary Figure 5h.

Reporting for specific materials, systems and methods

We require information from authors about some types of materials, experimental systems and methods used in many studies. Here, indicate whether each material, system or method listed is relevant to your study. If you are not sure if a list item applies to your research, read the appropriate section before selecting a response.

Materials & experimental systems

n/a	Involved in the study
☐	☒ Antibodies
☐	☒ Eukaryotic cell lines
☒	☐ Palaeontology
☐	☒ Animals and other organisms
☒	☐ Human research participants
☒	☐ Clinical data

Methods

n/a	Involved in the study
☒	☐ ChIP-seq
☒	☐ Flow cytometry
☒	☐ MRI-based neuroimaging

Antibodies

Antibodies used	anti-Centrin, clone 20H5, Millipore, 04-1624, mouse CEP164, EMD Millipore, ABE2621, rabbit Acetylated-alpha tubulin, Cell Signaling Technologies, 12152, mouse ZO-1, ThermoFisher Scientific, 14-9776-82, rat DEUP1 #1 homemade, raised against full-length mouse DEUP1, rabbit DEUP1, homemade, raised against the peptide TKLKQSRHI, rabbit γTubulin-555, homemade, raised against the peptide CDEYHAATRPDYISWGTQEQ, goat GT335, Adipogen, mouse SAS6, Santa Cruz, mouse Pericentrin, Covance, rabbit CEP63, Proteintech, rabbit
Validation	All of our homemade antibodies were validated by immunoblotting and immunofluorescence to ensure the loss of signal after RNAi depletion or CRISPR/Cas9 knockout of the target protein. When available, we purchased commercial antibodies that have been previously validated in multiple independent studies. In cases where this was not possible, commercial antibodies were validated in house in the same way we validate our homemade antibodies.

Eukaryotic cell lines

Policy information about cell lines

Cell line source(s)	DLD1 and HEK293FT cells were obtained from the lab of Don Cleveland and Carol Greider, respectively.
Authentication	Both cell lines were validated using STR Profiling at the Johns Hopkins Genetics Core Research Facility.
Mycoplasma contamination	All our cell lines used in the study were routinely checked for mycoplasma contamination by DAPI staining.

Commonly misidentified lines (See ICLAC register)	No commonly misidentified cell lines were used.

Animals and other organisms

Policy information about studies involving animals; ARRIVE guidelines recommended for reporting animal research

Laboratory animals	Laboratory mice (Mus musculus) were maintained on a congenic C57BL/6 background. Both male and female mice were used in this study. Mice were sacrificed at p0-p4 for ependymal cultures or at ~1-6 months old for tracheal epithelial cell cultures. Analysis of airway cilia and brain morphology was performed on adult mice of ~12 weeks of age.
Wild animals	N/A
Field-collected samples	N/A
Ethics oversight	Mice were housed and cared for in an AAALAC-accredited facility and experiments were conducted in accordance with Institute Animal Care and Use Committee approved protocols (for AJH), or in accordance with the guidelines of the European Community and French Ministry of Agriculture and were approved by the Direction départementale de la protection des populations de Paris (Approval number APAFIS#9343-201702211706561 v7) (for AM).

Note that full information on the approval of the study protocol must also be provided in the manuscript.